Dispersion State Study of Carbon Nanotube Epoxy Mixtures Using Linear and Nonlinear Rheology

By

Negin Moaseri

A thesis submitted to the Graduate Faculty of
Auburn University
in partial fulfillment of the
requirements for the Degree of
Master of Science

Auburn, Alabama
August 8, 2026

Keywords: Carbon nanotubes, Graphene Oxide, Epoxy nanocomposites, Dispersion state study, Nonlinear rheology

Approved by

Virginia A. Davis, Chair, Professor of Chemical Engineering
Tae-Sik Oh, Associate Professor of Chemical Engineering
Suhasini Gururaja, Associate Professor of Aerospace Engineering

Abstract

Carbon nanotube (CNT)-reinforced epoxy nanocomposites have attracted significant interest due to their potential applications in aerospace, electronics, and structural materials. To achieve the full potential of these nanocomposites, CNTs must be effectively dispersed within the epoxy matrix, as the dispersion state strongly influences network formation and overall material performance (1-3). Therefore, this study aims to provide a deeper understanding of the dispersion behavior of CNTs in epoxy resin through linear and nonlinear rheological characterizations.

In this research, epoxy mixtures containing different concentrations of single-walled carbon nanotubes (SWCNTs) were prepared using tip sonication to evaluate the rheological percolation threshold through linear and nonlinear rheological measurements complemented by optical microscopy imaging. In addition, an electric field was applied to align the SWCNTs in the epoxy matrix. The results demonstrated that nanotube alignment reduced the percolation threshold, enabling the formation of an interconnected network at lower SWCNT concentrations.

Furthermore, graphene oxide (GO) was incorporated into the SWCNT/epoxy systems to investigate the synergistic effects of combining one-dimensional (1D) and two-dimensional (2D) nanomaterials. Two SWCNT:GO ratios and two preparation methods were examined to evaluate their influence on the linear and nonlinear rheological behaviors of the mixtures. The results showed that nonlinear rheological analysis could distinguish between mixtures with similar linear rheological responses,

highlighting its sensitivity to differences in nanofiller dispersion and microstructural development.

Artificial Intelligence (AI) Use Disclosure Statement

In the preparation of this thesis, the following Artificial Intelligence (AI) tool was used: ChatGPT. These tools were used primarily to assist with language editing, including improving grammar and sentence structure. The author acknowledges full responsibility for the intellectual content of this work and has ensured that all AI-assisted sections have been reviewed and revised for accuracy and an appropriate academic style. All AI-generated content was reviewed and validated for relevance, appropriateness, and accuracy before incorporation into the final document to maintain the scholarly integrity of this research.

Digital Accessibility Disclosure Statement

In the preparation of this thesis, the following digital accessibility tools were used to ensure that this document complies with federal requirements: MATLAB, Python, and Excel. The author acknowledges full responsibility for the intellectual content of this work and has made a good faith effort to comply with digital accessibility requirements in publishing, wherein the nature of the content does not significantly change in order to do so. Furthermore, all content has been reviewed and revised to meet these requirements prior to final publication.

Acknowledgments

I would like to express my sincere gratitude to my advisor, Dr. Virginia A. Davis, for her guidance, and support throughout my time at Auburn University. I am truly grateful for the opportunity to be a member of her research group and for the valuable experience I have gained under her mentorship.

This work would not have been possible without the collaboration and assistance of Dr. Suhasini Gururaja and Dr. Julkarnyne M. Habibur Rahman. I am grateful for the opportunity to work on this project. Dr. Rahman contributed significantly to this research by performing the carbon nanotube alignment process, curing the nanocomposites, and conducting the mechanical testing of the nanocomposite samples.

I would also like to thank my other thesis committee member, Dr. Tae-Sik Oh, for serving on my committee. In addition, I sincerely appreciate the members of the Davis Research Group for their assistance, collaboration, and support throughout this work.

Finally, I would like to thank my family, and friends for their unwavering encouragement, patience, and support during the past two years. Their belief in me has been invaluable throughout this journey.

Table of Contents

List of Tables

List of Figures

List of Abbreviations

CNT	Carbon Nanotube
SWCNT	Single-Walled Carbon Nanotube
GO	Graphene Oxide
1D	One-Dimensional
2D	Two-Dimensional
AC	Alternating Current
SEM	Scanning Electron Microscopy
MWCNT	Multi-Walled Carbon Nanotube
G′	Storage Modulus
G″	Loss Modulus
SAOS	Small Amplitude Oscillatory Shear
LAOS	Large Amplitude Oscillatory Shear
FT	Fourier Transform
FT-Rheology	Fourier Transform Rheology
L-B	Lissajous–Bowditch
SPP	Sequence of Physical Processes
AFM	Atomic Force Microscopy
PVP	Polyvinylpyrrolidone
DI	Deionized Water
TGA	Thermogravimetric Analysis
UV	Ultraviolet
LVR	Linear Viscoelastic Region
MAOS	Medium Amplitude Oscillatory Shear
ASTM	American Society for Testing and Materials
wt%	Weight Percent
vol%	Volume Percent
TiO_2	Titanium Dioxide
φc	Percolation Threshold
R^2	Coefficient of Determination
S	Strain-Stiffening Ratio
T	Shear-Thickening Ratio
I_3/I_1	Ratio of Third Harmonic Intensity to First Harmonic Intensity

Chapter 1: Introduction

Epoxy resin is the most widely used thermoset resin in reinforced polymer composites due to its many attractive properties, including high stiffness and good adhesion with other substrates (3). Various microscale and nanoscale fillers have been added to epoxy resins to further improve their mechanical properties in the fabrication of reinforced polymer composites. Although microscale fillers, such as carbon and glass fibers, can enhance the properties of the resin, they have some disadvantages, including the requirement of a high filler content for property improvement, which could increase the weight of the composite (4). Therefore, nanoscale materials such as carbon nanotubes and nanoclays have been used to overcome the challenges associated with the use of microscale fillers (5).

Carbon nanotubes (CNTs) are one-dimensional (1D) nanostructures that have been widely used as reinforcements in epoxy nanocomposites owing to their excellent properties. Carbon nanotube epoxy nanocomposites have been used in a wide range of applications, including the aerospace, automobile, and electronics industries. The combination of low density, high tensile strength, high Young's modulus, and high electrical conductivity have made CNT/epoxy nanocomposites, attractive materials for advanced engineering applications. (3, 6, 7). However, CNTs tend to form aggregated clusters owing to the strong van der Waals forces between them. These aggregated clusters can reduce the mechanical, electrical, and thermal properties of the nanocomposites (8-10). Therefore, the dispersion state of carbon nanotubes in epoxy resin plays a major role in the properties of epoxy nanocomposites (11, 12).

This study probes the dispersion state of CNTs in epoxy resin using rheology. Rheology is a powerful tool for studying the dispersion state of nanomaterials in polymer matrices (8, 9). Furthermore, graphene oxide (GO) is added to the system to study the dispersion state of 1D and 2D nanomaterials in the epoxy matrix. The objectives of this study are as follows:

Objective 1) Studying the dispersion state of single-walled carbon nanotubes in epoxy resin, using rheology and microscopy imaging

Objective 2) Alignment of CNTs in the epoxy matrix using an AC electric field (In collaboration with Dr. Gururaja's group)

Objective 3) Study the effect of the addition of GO as a secondary nanofiller on the dispersion state of SWCNT epoxy mixtures using linear and nonlinear rheology

Carbon nanotubes (CNTs) are classified into single-walled (SWCNTs) and multi-walled (MWCNTs), each providing distinct benefits in polymer-based composites. SWCNTs, consist of a single rolled graphene layer, whereas MWCNTs are composed of multiple concentric graphene layers (13). Due to their superior mechanical and electrical characteristics and high aspect ratio, CNTs can enhance properties at very low filler loadings, making them highly suitable for advanced multifunctional applications (14, 15). In this study, SWCNTs were dispersed in an epoxy resin using ultrasonication to achieve a uniform dispersion throughout matrix. A well-dispersed network facilitates the formation of an interconnected nanotube system as the SWCNT concentration increases. The minimum filler content at which this continuous path is formed is referred to as the percolation threshold of SWCNTs in the matrix (13, 16).

The alignment of the nanofillers is a key factor in achieving SWCNTs' anisotropic properties in macroscale systems. Applying external forces, such as shear, electric (17-23) and magnetic fields (24-26), is an effective method for aligning CNTs. The application of an electric field has been widely used for the alignment of CNTs because of the high electrical conductivity of CNTs and the low cost of the experimental setup (17, 18). Optimizing different parameters, such as the electrode distance, and voltage plays a critical role in the alignment of CNTs (27, 28). In this study, an alternating current (AC) electric field was used to align SWCNTs in epoxy resin. Additionally, several characterization tests, including Raman mapping and scanning electron microscopy (SEM), were performed to study the alignment of the SWCNTs in the epoxy resin.

In addition to CNTs, members of the graphene family, which share a similar molecular structure but possess a two-dimensional (2D) sheet-like morphology, have also been widely investigated as reinforcing nanofillers. Graphene oxide (GO) is a two-dimension (2D) structure that has been used as reinforcement in the epoxy composites due to its outstanding properties such as high thermal conductivity and large specific surface area (29, 30). Many studies have investigated the synergistic effect of CNTs and GO on the properties of nanocomposites (12, 31-33). However, to the best of our knowledge, no study has investigated the nonlinear rheology of CNTs and GO in an epoxy matrix.

Chapter 2: Background

Carbon nanotubes' structure

The discovery of carbon nanotubes is typically attributed to Iijima in 1991. There are two primary types of carbon nanotubes: single-walled carbon nanotubes (SWCNTs) and multi-walled carbon nanotubes (MWCNTs). SWCNTs consist of only one graphite cylinder and typically have a diameter of approximately 1 nm. Similarly, MWCNTs consist of coaxial cylinders of graphene with an outer diameter of 2-20 nm (13, 34).

The chirality of a carbon nanotube describes how a graphene sheet is wrapped to form a cylindrical structure. It is defined by a pair of integers, (n, m) which specify the circumferential chiral vector C_h and determine the geometrical configuration of the rolled graphene sheet. Where $\overrightarrow{C_h}$:

$$\overrightarrow{C_h} = n\overrightarrow{a_1} + m\overrightarrow{a_2} \qquad (1)$$

The cylinder connecting the hemispherical caps of the nanotube is formed by superimposing the two ends of vector C_h, and the joint is formed by the two lines OB.

Zigzag nanotubes are characterized by index pairs $(n, 0)$ or $(0, m)$, while armchair nanotubes correspond to the (n, n) configuration (Figure 1). Because these two geometries contain a mirror plane, they are considered achiral, whereas all other (n, m) index pairs give rise to chiral structures. Variations in both the chiral angle and tube diameter lead to differences in their physical properties. Nanotubes for which n-m is divisible by three exhibit metallic behavior; otherwise, they are semiconducting.

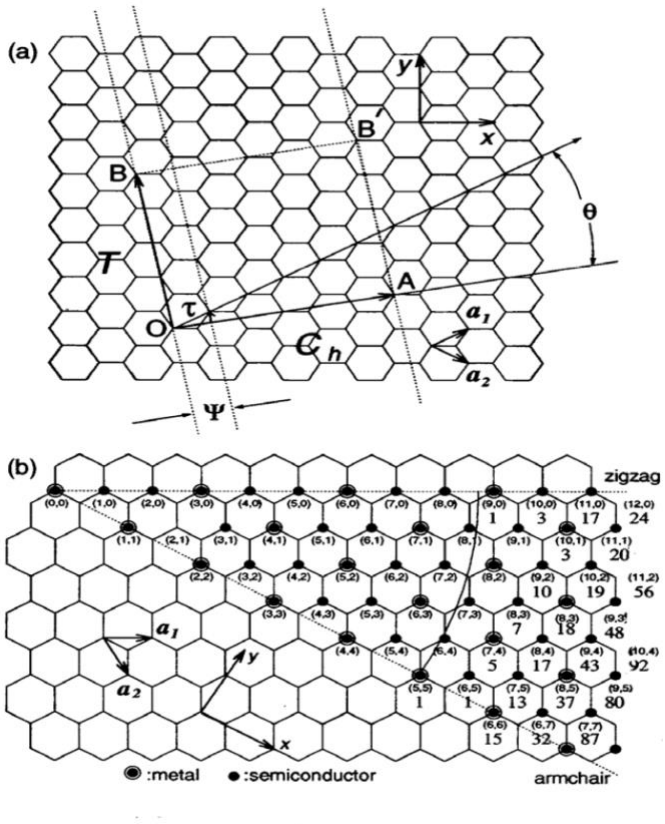

Figure 1. a) Honeycomb of a graphite sheet, a1 and a2 are the unit vectors and θ is chiral angle. In the zigzag orientation, θ is equal to zero. The lattice vector of the 1D nanotube unit cell, OB = T, is also depicted. The basic symmetry of the nanotube is determined by the rotation angle ϕ and translation τ. b) Vectors for the formation of different nanotube structures. Metallic and semiconducting nanotubes are shown with encircled and single dots, respectively (34).

Armchair and zigzag carbon nanotubes are classified as achiral because they possess mirror plane symmetry. In contrast, nanotubes with chiral vectors, where n is not equal to m and neither index is zero, lack this symmetry and are therefore considered chiral. The nanotube diameter is calculated from the chiral indices using

$$d = \frac{\sqrt{3}a\sqrt{m^2+mn+n^2}}{\pi} = \frac{C_h}{\pi} \qquad (2)$$

Where a is the carbon bond length, approximately 1.42 nm for graphite. This equation shows the relationship between tube diameter and the magnitude of C_h. The figure below shows the three different structures of carbon nanotubes (34).

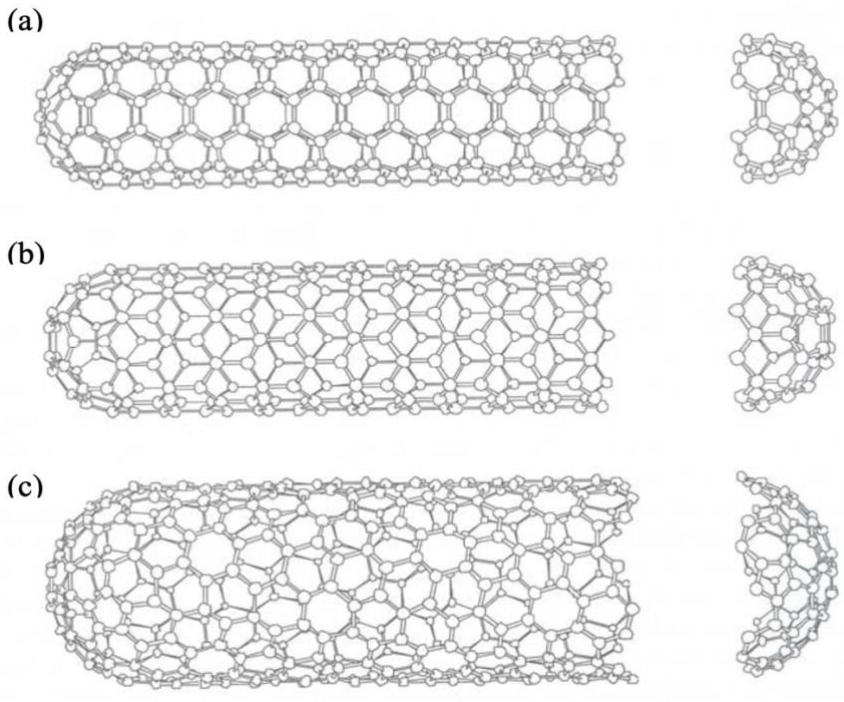

Figure 2. Schematic theoretical model for a SWCNT with a) an armchair, b) zigzag, and c) chiral structures (34).

Intermolecular potential in CNT/epoxy mixtures

The interactions between dispersed nanomaterials are commonly described by Derjaguin, Landau, Verwey, and Overbeek (DLVO) theory, which considers the balance between attractive and repulsive forces governing colloidal stability. The total interparticle potential arises from the combined influence of van der Waals attractions, electrostatic repulsions, depletion interactions, and sedimentation effects, which collectively affect the dispersion state of the nanoparticles (35, 36).

van der Waals forces occur between two neutral molecules that have no net charge or permanent dipole moment. As two molecules move closer together, the van der Waals interactions initially become more attractive, reaching their strongest point at an intermediate distance from each other. However, when the molecules become too close, these interactions shift and become strongly repulsive. The van der Waals radius is defined as half of the separation distance between two identical atoms when they are positioned in the minimum energy state (Figure 3) (2, 37). Due to the highly polarizable sp^2-hybridized carbon structure of carbon nanotubes, SWCNTs exhibit a strong tendency to form bundles and agglomerates. These aggregates are held together by significant van der Waals attractions, with strengths on the order of 20–40 K_bT/nm (35).

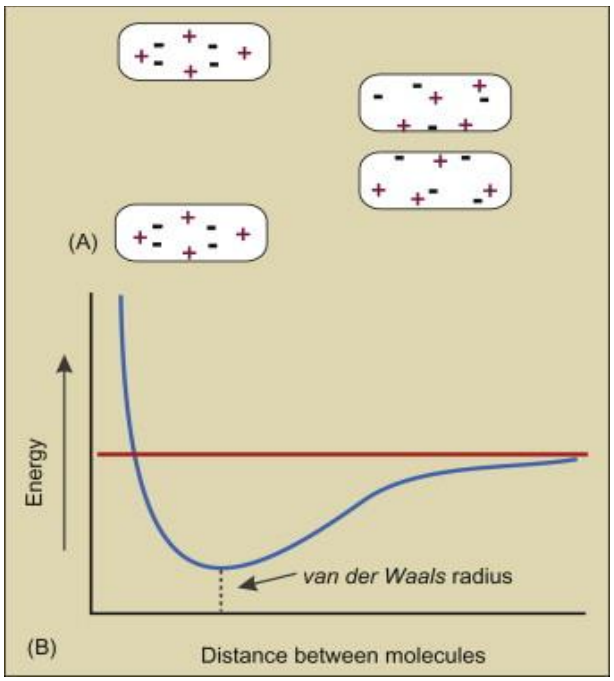

Figure 3. (A) Temporary charge fluctuations generate van der Waals attractions between the neutral molecules. B) These forces increase with decreasing separation, reach a maximum value, and become repulsive at short distances (2).

GO structure

Graphene oxide (GO) is a two-dimensional nanostructure obtained through the chemical oxidation and exfoliation of graphite layers. During the chemical exfoliation process, numerous oxygen functional groups are introduced onto the two-dimensional carbon lattice of the GO. These functionalities commonly include epoxide bridges, carbonyl (C=O) groups, hydroxyl (–OH) and phenolic species, and organ sulfate groups that may be present due to sulfur-related impurities (38, 39).

Figure 4 shows the timeline of GO synthesis. Brodie first documented the oxidation of graphite in 1859, marking one of the earliest systematic attempts to chemically modify graphite. Prior to this work, Schafhäeutl demonstrated graphite intercalation in 1840, providing an important foundation for subsequent oxidation-based approaches (40). In 1898, Staudenmaier introduced an improved synthesis route that relied on a combination of nitric and sulfuric acids with potassium chlorate, offering a procedure that was safer and less labor-intensive than Brodie's method. Although these early techniques advanced the understanding of graphite chemistry, the method developed by Hummers and Offeman in 1958, using a mixture of sulfuric acid, sodium nitrate, and potassium permanganate, gained widespread acceptance owing to its relative efficiency, reduced reaction time, and improved reproducibility (41). Consequently, the Hummers method and its numerous modifications remain the most widely employed approaches for producing graphene oxide today (42).

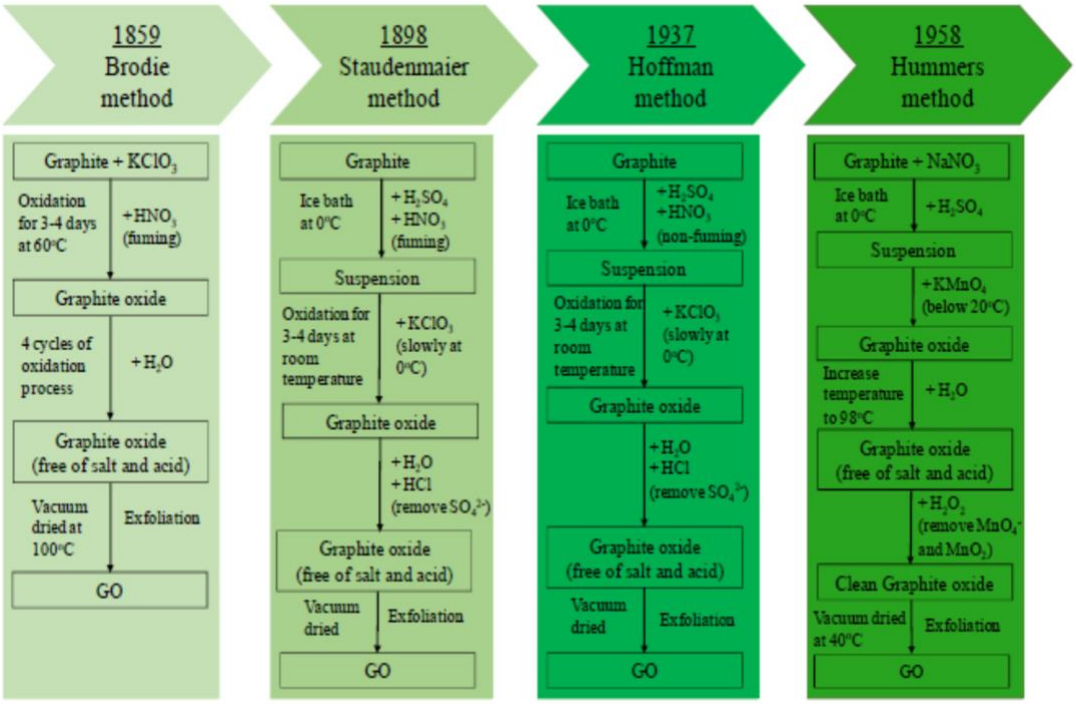

Figure 4. Timeline of GO synthesis (39).

Nanofiller epoxy nanocomposites

Epoxy nanocomposites can be classified into two different groups based on the morphology of their nanofillers. The first group includes isotropic nanofiller-reinforced epoxy nanocomposites, including titanium dioxide (TiO_2) and nano-alumina epoxy nanocomposites. Isotropic nanofillers are identified as materials with identical dimensions in all directions, such as spherical particles. Conversely, anisotropic materials exhibit different physical properties along different directions or axes. Following the discovery of carbon nanotubes, the morphology and shape of nanofillers have been recognized as key factors for enhancing the properties and performance of nanocomposites (43).

Several processing methods have been developed for the preparation of polymer nanocomposites, including mechanical mixing, and in situ polymerization. Mechanical

mixing combined with solvent intercalation is widely used for dispersing nanomaterials with high aspect ratios, such as carbon nanotubes in thermoset resins. In this method, the nanomaterials and polymer matrix are initially dispersed in separate solvent suspensions, and after mixing, the solvent is removed through evaporation, leaving a mixture with improved filler dispersion (44). In addition, the in-situ polymerization method is a widely used technique for making polymer nanocomposites. In this method, nanofillers are first dispersed in the neat monomer, followed by the addition of an initiator, and finally, the mixture is exposed to a source of heat (45). Figure 5 shows a schematic of this method.

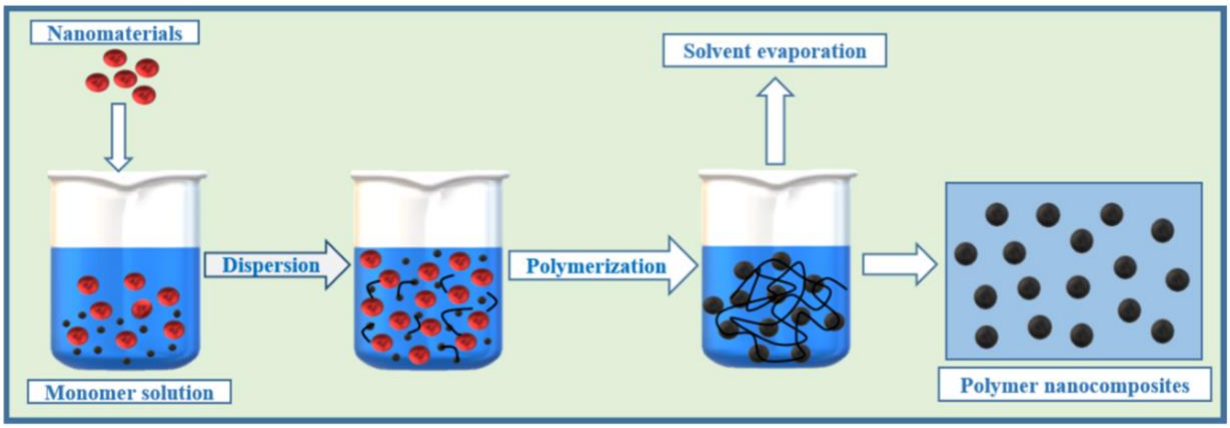

Figure 5. Schematic of the in-situ polymerization method (46).

Nonlinear Rheology

Rheological characterization can be performed using two primary testing methods: steady shear rheology and oscillatory rheology. In steady shear rheology, a constant shear rate or shear stress is applied to the sample to measure its flow behavior, such as viscosity as a function of shear rate. In contrast, oscillatory rheology

applies a sinusoidal shear strain or shear stress to the sample to probe its time-dependent viscoelastic response. Oscillatory rheology can be studied in two different regimes. The linear viscoelastic regime, where the storage modulus (G') and loss modulus (G'') are independent of strain, and the resulting stress response exhibits a purely sinusoidal waveform. In contrast, the nonlinear regime, where both the storage and loss moduli depend on strain, and the stress response deviates from a sinusoidal shape (47) (Figure 6).

In many industrial applications and processes, epoxy nanocomposites undergo rapid deformation. Therefore, understanding their response in the nonlinear regime could help us simulate the processing better (47, 48).

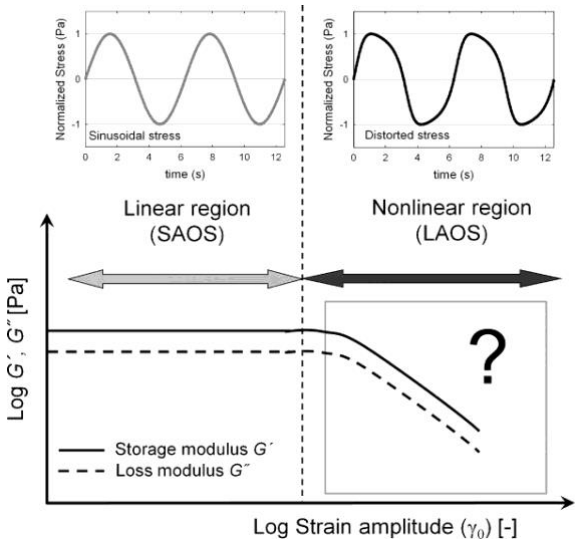

Figure 6. Schematic illustration of the SAOS and LAOS regimes in the amplitude sweep test (47).

In LAOS, unlike SAOS, the rheological material functions cannot be fully interpreted by G' and G''. Hence, rheologists have developed various methods to analyze LAOS results, including Fourier-transform rheology, Lissajous-Bowditch (L-B)

curve analysis, and sequence of physical processes (SPP). Figure 7 shows the timeline of the different LAOS techniques (48).

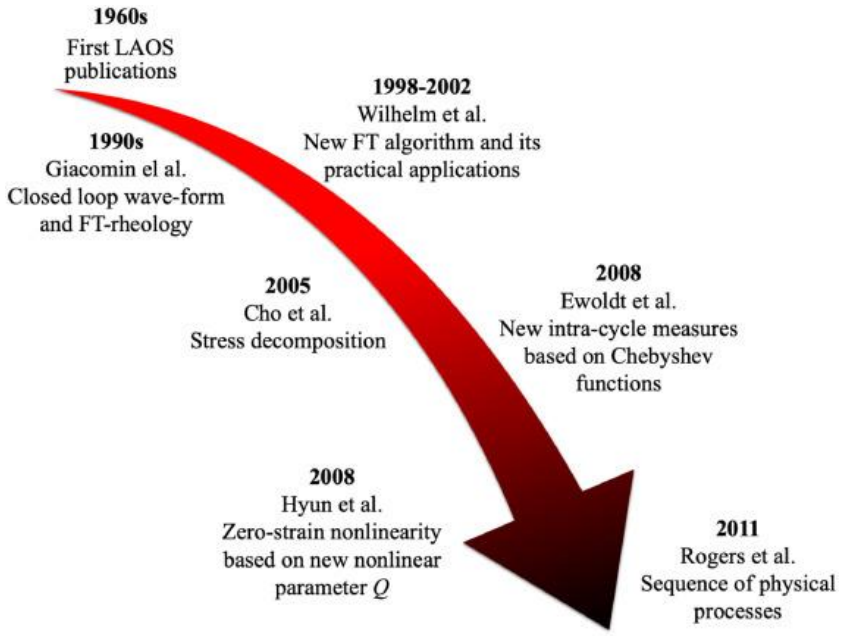

Figure 7. Timeline of LAOS techniques (49).

As mentioned earlier, as the strain amplitude increases, the stress response deviates from a purely sinusoidal waveform, indicating the onset of nonlinear viscoelastic behavior (48). Fourier Transform (FT) rheology characterizes this nonlinear response by decomposing the stress signal into a series of harmonic contributions. In FT rheology, only odd harmonics are considered under the assumption that the stress response is an odd function of the applied strain. Whereas the first harmonic dominates in the linear regime, the third and higher-order harmonics become increasingly significant in the nonlinear regime. Therefore, the intensity ratio of the third to the first harmonic is commonly used to identify the onset of nonlinear behavior (49).

Although the ratio of odd harmonic peaks is commonly used to distinguish materials with different microstructures, it does not provide a direct physical interpretation. To address this, Cho et al. proposed an orthogonal stress decomposition model based on the Fourier series by determining the generalized storage and loss moduli (50).

Although the introduction of the Chebyshev function in 2008 helped address some of the limitations associated with the direct Fourier series approach, there were still some limitations in interpreting the material deformation state (51). Rogers et al. introduced a sequence of physical processes (SPP) analysis that allows the specification of the transient modulus and viscosity within the oscillation. In this technique, the Frenet–Serret framework is employed to describe the position of a point in three-dimensional space using a set of vectors comprising the tangent vector (T(t)), normal vector (N(t)), and binormal vector (B(t)). This approach not only provides better physical insight into the material response throughout the oscillatory cycle across all strain amplitudes, but also The SPP technique enables a comprehensive analysis of the complex interactions and interpenetration behavior between the two surfaces (49, 51-53).

Chapter 3: Materials and experimental details

Preparation CNT epoxy mixtures

Single-walled carbon nanotubes (SWCNTs) and graphene oxide powders were purchased from OCSiAl (Tuball, 01RW02) and William Blythe (JC05-184JP), respectively. The epoxy resin system consisted of Epon-862 (diglycidyl ether of bisphenol F) and EPIKURE curing agent W (bisphenol-F epoxy resin and an aromatic amine), both of which were procured from Miller-Stephenson. To prepare a 0.03 wt% SWCNT/epoxy mixture, 12 mg of SWCNTs were added to 40 g of epoxy resin. The mixture was then ultrasonicated at 60% amplitude for 40 min (power of 750 W, frequency of 20 kHz) to achieve a uniform dispersion of the SWCNTs in the epoxy resin. An ice bath was used during sonication to avoid overheating.

Since volume fraction determines percolation, the volume fraction of nanomaterials in epoxy (ϕ) was calculated using the density of nanomaterials (ρ_n) and the density of epoxy resin (ρ_r) in equation below:

$$\phi = \frac{\frac{m_n}{\rho_n}}{\frac{m_n}{\rho_n}+\frac{m_r}{\rho_r}} \qquad (3)$$

where m_n and m_r are the masses of the nanomaterials and epoxy resin, respectively. Table 1 shows the varying SWCNT concentrations.

For curing rheology, the curing agent (Epikure W) was added to the mixtures at a mixing ratio of (100:26.4) and stirred on a hot plate for 5 min at room temperature. Then,

the mixtures were vacuum degassed to remove air bubbles. To make nanocomposite, the mixture was then poured into a preheated aluminum mold (made according to ASTM D638 Type I) and placed in an oven. The curing process was conducted at 121°C for 2 h, followed by 177°C for 2 h.

Table 1. Different concentrations of SWCNT/epoxy mixtures

SWCNT Concentration (wt%)	0.020	0.030	0.040	0.050	0.070	0.100	0.150
SWCNT Concentration (vol%)	0.012	0.019	0.025	0.031	0.043	0.062	0.093

Alignment of SWCNTs in the epoxy resin

To align the SWCNTs within the epoxy matrix, an alternating current (AC) electric field with a voltage of 500 V and frequency of 10 kHz was applied using a function generator connected to a power amplifier. The mixture was maintained at 80°C before being transferred into a preheated silicone mold measuring 90 mm × 350 mm (L × W). Copper electrodes were positioned at a fixed distance of 10 mm to cover the gauge length region (50 mm) of the mold, which was selected to match the length of the extensometer. Custom 3D-printed holders were used to secure the electrodes during the alignment process. After curing, the nanocomposite plates were cut into ASTM D638 Type I specimens using a Wazer Desktop waterjet. Using this procedure, SWCNT/epoxy nanocomposites containing 0.03, 0.05, and 0.07 wt% SWCNTs were

fabricated in this study. This part of the research was done by Dr. Julkarnyne M Habibur Rahman in Dr. Suhasini Gururaja's group.

Preparation SWCNT-GO epoxy mixtures

Two different dispersion methods (Methods A and B) were employed to prepare 0.2 wt% SWCNT/GO epoxy mixtures with two different ratios. Method A involved a straightforward approach, similar to that used for preparing the SWCNT-epoxy mixture. In this method, both SWCNTs and GO were added directly to the epoxy resin. The mixture was then subjected to tip sonication for 10 min at 60% amplitude to facilitate the dispersion of the nanofillers.

Method B followed a solvent intercalation procedure: first, ethanol was used as a solvent to disperse the GO flakes. The SWCNTs were separately dispersed in the epoxy resin using tip sonication. Subsequently, the GO-ethanol mixture was combined with the SWCNT-epoxy mixture, and high-shear mixing was performed for 3 h to ensure uniform dispersion. Finally, the mixture was placed in a vacuum oven overnight to remove any residual solvent by degassing.

Table 2. Composition of SWCNT-GO epoxy mixtures.

Sample	Method	SWCNT:GO	Concentration (wt%)		
			SWCNT	GO	Epoxy
A-1:1	A	1:1	0.10	0.10	99.8
A-1:3	A	1:3	0.05	0.15	99.8
B-1:1	B	1:1	0.10	0.10	99.8
B-1:3	B	1:3	0.05	0.15	99.8

Atomic Force Microscopy

To measure the dimensions of the nanomaterials, an Anton Paar Tosca 400 Atomic Force Microscope (AFM) was used in tapping mode. To measure the dimensions of the SWCNTs, 10 mg of SWCNTs were added to 20 ml of 1% PVP aqueous solution and sonicated using tip sonication (25% amplitude) for an hour. To measure the GO nanoparticles, a 0.5 $mg.ml^{-1}$ dispersion of GO and DI water was prepared using bath sonication for 20 min. The mixtures were then drop-cast onto freshly cleaved mica and dried at room temperature. All images were processed using the Tosca Analysis software.

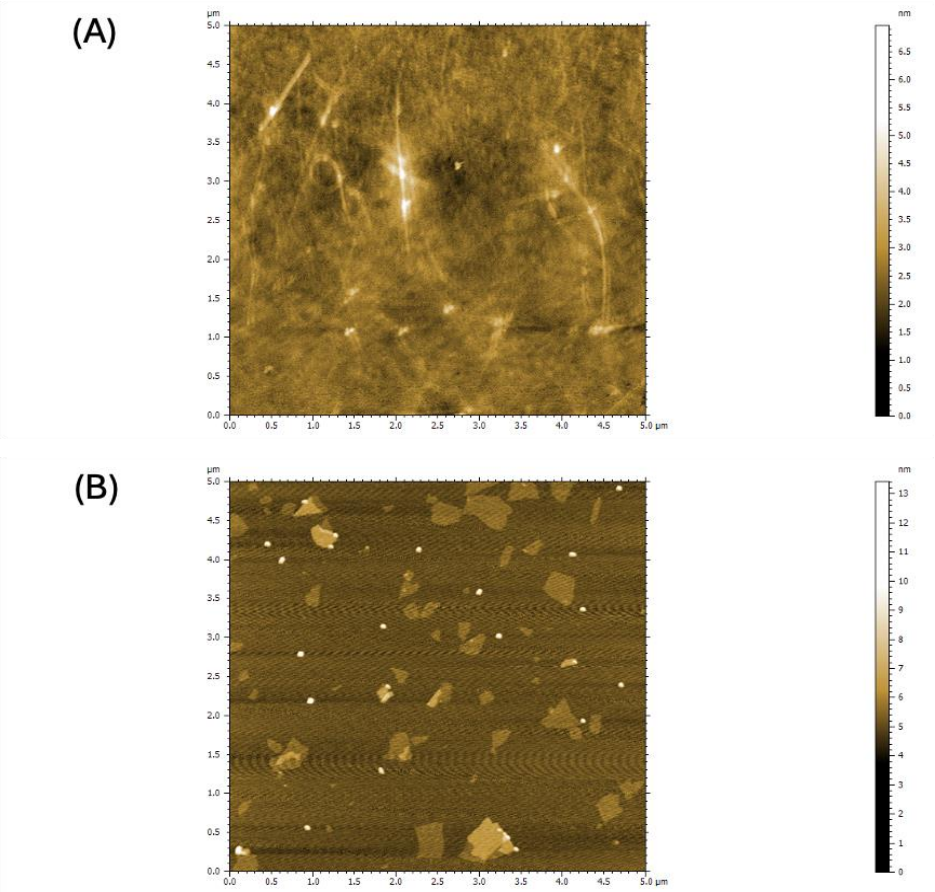

Figure 8. AFM images of A) single-walled carbon nanotubes (SWCNT) B) graphene oxide (GO).

Raman Spectroscopy

Raman spectra were acquired using a Renishaw *inVia* Raman microscope equipped with a 50X objective lens. Raman spectra were acquired using two wavelengths (532 and 785 nm), with measurements collected from three different spots using a 10 s exposure time and laser powers of 0.1% and 0.5%.

Raman maps were obtained using a Renishaw *inVia* Raman microscope equipped with a 50× objective lens using a 785 nm laser. A step size of 10 μm, exposure time of 1 s, and three accumulations were applied for each measurement.

Thermogravimetric Analysis

The purity and thermal stability of the nanomaterials were evaluated using thermogravimetric analysis (TGA) with a TA Instruments Q500 system in air and nitrogen. The temperature was initially held at 25 °C for 30 min, then increased at a rate of 10 °C min^{-1} to 130 °C, and maintained for 30 min. Subsequently, the temperature was increased to 800 °C at a rate of 10 °C min^{-1} and held for 45 min.

Dispersion rheology

Linear rheological measurements of the mixtures were performed using an Anton Paar MCR 301 rheometer with a 50 mm parallel plate geometry. All tests were conducted at 25 °C. The sample was left to sit undisturbed for an hour after loading to stabilize. The following procedures were followed:

1- An amplitude sweep test was performed at a frequency of 10 rad/s.
2- A frequency sweep was performed at the critical strain from 0.1 to 100 rad/s angular frequency. Subsequently, amplitude and frequency sweep tests were repeated using the same parameters.
3- Step rate test was performed at 0.1 s^{-1}.
4- The flow curve test was performed at shear rates of 0.01-100 s^{-1}.

Curing rheology was performed at 120 °C using disposable parallel plates (50 mm diameter). A constant strain amplitude of 5% and an oscillation frequency of 1 Hz were applied throughout the measurements to monitor the evolution of the viscoelastic properties during the curing process.

Nonlinear Rheology

For nonlinear rheology, a large amplitude oscillatory shear (LAOS) test was performed using an Anton Paar Physica MCR 302e strain-controlled rotational rheometer. All the tests were performed on a 50 mm parallel-plate fixture and at the temperate of 25 °C. An amplitude sweep was performed at 0.8 rad/s from 0.01% to 1000%, with the raw waveform collected simultaneously.

The raw waveform data collected at each strain amplitude were analyzed using MATLAB-based Sequence of Physical Processes (SPP) software. The time, strain, strain rate, and stress data were processed using Fourier domain filtering to reconstruct the signal using all detectable odd harmonics above the noise level.

Optical Microscopy

To evaluate the dispersion state, optical microscopy was performed using a Nikon Eclipse 80i microscope operating in transmission mode, equipped with a Nikon DS-Ri2 digital camera, and controlled by Nikon Elements software. Imaging was performed using a 20×/0.45 objective lens. A small drop of the nanomaterial–epoxy mixture was placed on a clean glass slide and covered with a cover slip.

Scanning Electron Microscopy (SEM)

A JEOL JSM-7000F scanning electron microscope was used to assess the microstructure and alignment of the nanomaterials inside the epoxy resin. For sample preparation, the fractured surfaces of the composites were mounted onto aluminum SEM stubs using carbon adhesive tape. A thin line of silver paint was applied between

the sample surface and the stub to minimize the charging. Prior to imaging, all samples were sputter-coated with a thin gold layer.

Chapter 4: Results and Discussion

Characterization of SWCNTs and GO

In Raman spectroscopy, the sample is exposed to an intense laser source, and the scattered light is collected to analyze the vibrational characteristics of the material. This technique is widely used to characterize the structural properties of carbon-based nanomaterials, including carbon nanotubes and graphene. The D-band, typically observed at approximately 1350 cm^{-1}, is associated with structural defects and sp^3 hybridized carbons. On the other hand, the G-band is located around 1595-1610 cm^{-1} and is related to sp^2 carbon structure (54). The intensity ratio of the D band to the G band is widely used to evaluate the degree of disorder in carbon materials. This disorder may result from lattice defects or from intentional or unintentional functionalization. Additionally, radial breathing modes (RBMs), typically observed in the range of 100–500 cm^{-1}, are characteristic features of single-walled carbon nanotubes (SWCNTs) and serve as the evidence of their presence. RBMs originate from the collective radial vibration of carbon atoms, causing the nanotube diameter to periodically expand and contract in a breathing-like motion (55).

Table 3 summarizes the Raman spectroscopy and TGA results for the nanomaterials. The SWCNTs exhibited low I(D)/I(G) intensity ratios for both the 532 nm (mostly sensitive to metallic nanotubes) and 785 nm (mostly sensitive to semiconducting nanotubes) excitation lasers, indicating a low defect density and a well-ordered graphitic structure. These results suggest that the SWCNTs possessed a high structural quality. In contrast, GO exhibited different behaviors depending on the laser

wavelength. Although a relatively low I(D)/I(G) ratio was observed with the 532 nm laser, the Raman spectrum obtained using the 785 nm laser exhibited a higher D-band intensity than the G-band. This increase in the D-band could be attributed to a higher degree of structural disorder and the presence of amorphous carbon and residual impurities within the GO structure.

Table 3. Raman and TGA results of the nanomaterials.

Nanomaterial	Raman		TGA	
	D/G 532 nm	D/G 785 nm	Residue N_2 (wt%)	Residue Air (wt%)
SWCNT	0.040	0.140	89.5	17.7
GO	0.850	1.45	32.5	1.39

Thermogravimetric analysis (TGA) was performed to measure the thermal stability of the nanomaterials. While performing TGA in an N_2 environment can provide information about the thermal decomposition of nanomaterials, conducting TGA in an air atmosphere evaluates the oxidative stability and purity of the materials. According to Table 3, GO show better thermal stability and fewer impurities than SWCNTs.

Rheological characterization of SWCNTs in the epoxy resin

Oscillatory shear measurements provide valuable insights into the microstructure and viscoelastic behavior of material systems. The storage modulus (G') represents the elastic or solid-like response of the material and reflects the energy stored during deformation, whereas the loss modulus (G'') characterizes the viscous behavior of the material and indicates the amount of energy lost during deformation (1, 56).

The viscoelastic behavior of mixtures has been used to study the dispersion state and determine the percolation threshold of SWCNTs. Percolation threshold (ϕ_c) is the minimum filler content that forms a continuous path of fillers in the matrix (35). Several methods have been proposed in the literature for estimating percolation. Using the frequency sweep (G' and G'' versus frequency) plots is the simplest way to find a first approximation for ϕ_c (1, 56).

Figure 9 displays G' and G'' versus angular frequencies for different SWCNT concentrations. As can be seen, there is a jump in G' and G'' between 0.05 and 0.1 wt%. This could suggest a presence of a weak percolation network that may have formed between these concentrations. However, the increase in G' is less than one order of magnitude, and the storage modulus remains frequency-dependent even at the lowest frequencies measured. These characteristics indicate that none of the dispersions have reached the rheological percolation threshold necessary to form a continuous CNT network. To estimate a more accurate percolation threshold, the power law relation $G'_0 \propto (\emptyset - \emptyset_c)^{\beta}$ has been performed by adjusting ϕ_c to have the highest R^2. Figure 8C shows the low-frequency storage modulus G'_0 of the SWCNT-epoxy mixtures. Based on this

method, the ϕ_c ~ 0.05 wt% which is consistent with ϕ_c ~R/L of SWCNTs (0.05 wt%) (1, 56, 57).

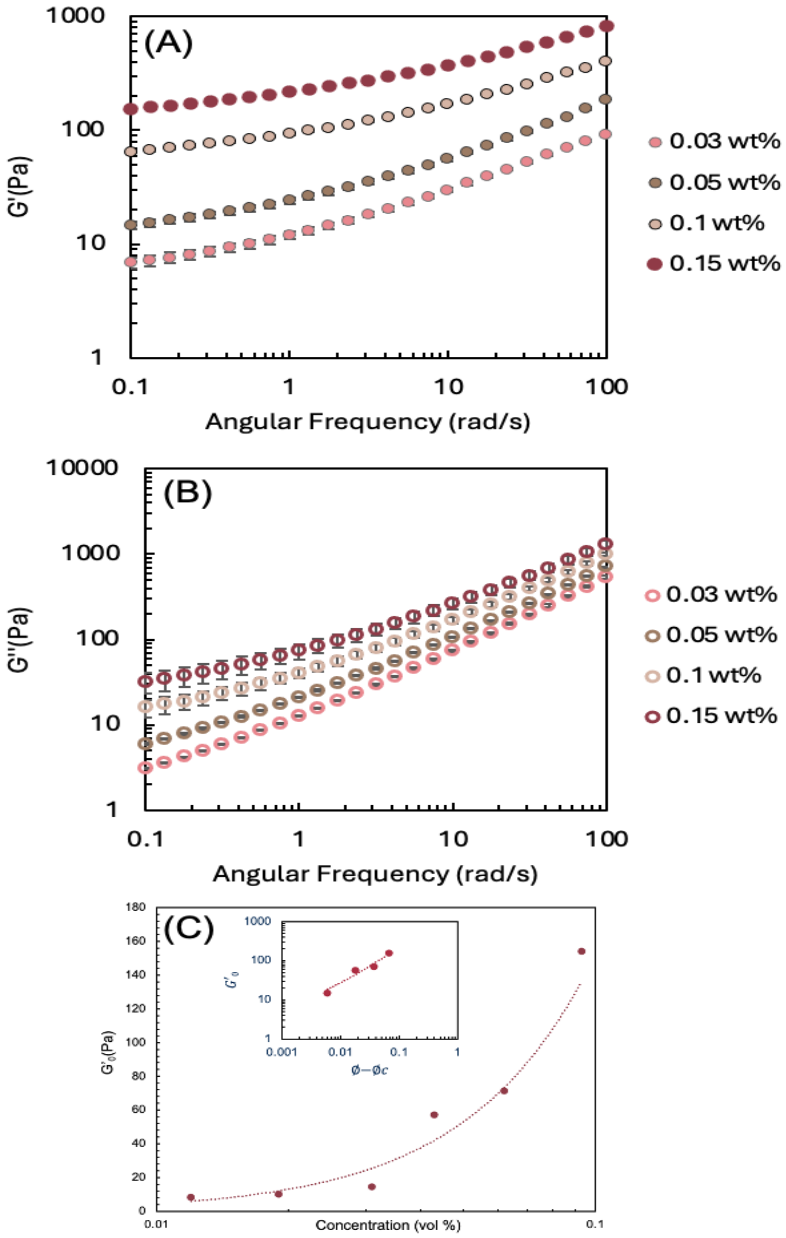

Figure 9. Oscillatory shear rheology curves of A) G' and B) G'' as a function of angular frequency. C) Low-frequency storage modulus versus concentration of SWCNTs. The solid line shows the fit to a power law.

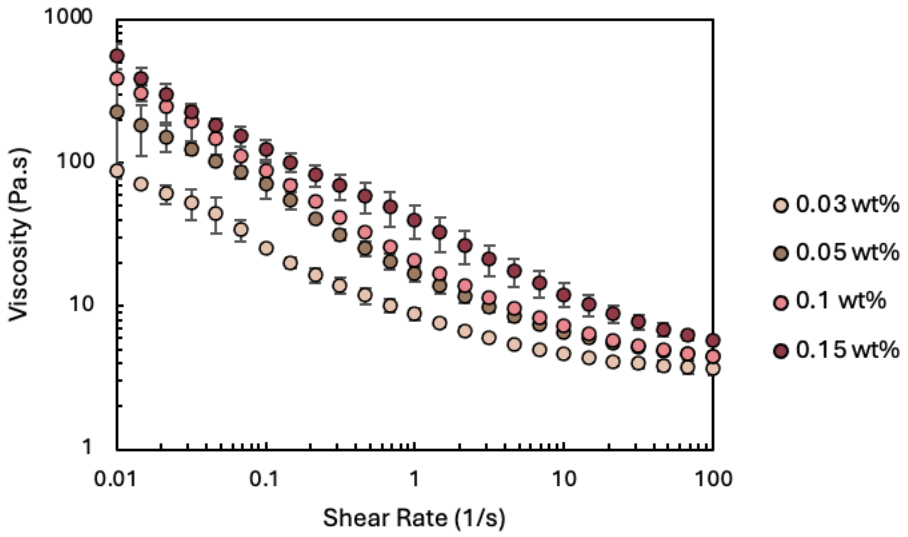

Figure 10. Viscosity of SWCNT/epoxy mixtures as a function of shear rate.

Figure 10 shows the flow curves of the SWCNT Epoxy mixtures at different concentrations. Increasing the concentration of SWCNT increased the viscosity of the mixtures, mostly at low shear rates. The Carreau-Yasuda (58, 59) and Herschel–Bulkley (60) models were used to fit the experimental data to evaluate the shear-thinning behavior of the mixtures. The Carreau-Yasuda model is as follows:

$$\eta\ (\dot{\gamma}) = \eta_{\infty} + (\eta_0 - \eta_{\infty})\ [1+(\lambda\dot{\gamma})^{\alpha}]^{\frac{n-1}{\alpha}} \qquad (4)$$

Where η is the viscosity, and $\dot{\gamma}$ is the shear rate.

Based on the model mentioned above, Table 4 lists the definitions of each parameter and the values of the parameters for each concentration.

Table 4. Summary of the Carreau-Yasuda model parameters.

Parameters		Concentrations (wt %)			
		0.030	0.050	0.100	0.150
η_0	Zero-shear Viscosity	189	239	772	625
η_∞	Infinite-shear Viscosity	4.00	0.617	4.00	13.0
λ	Characteristic Time Constant	87.8	110	221	125
a	Empirical Transition Parameter	0.670	11.5	1.44	76.4
n	Power-law Index	0.160	0.460	0.290	0.290
R^2		0.998	0.998	0.999	0.993

Equations 3 and 4 provide the Herschel-Bulkley model in terms of stress and viscosity, respectively.

According to the Herschel-Bulkley model:

$$\sigma = \sigma_y + K\dot{\gamma}^n \qquad (5)$$

$$\eta = \eta_o + K\dot{\gamma}^{n-1} \qquad (6)$$

where n, K, σ_y and η_o are the flow index, consistency index, yield stress and viscosity at yield stress respectively. Table 5 shows the parameters of this equation for different

concentrations of SWCNT epoxy mixtures. Although both the Herschel–Bulkley and Carreau–Yasuda models provided excellent fits to the experimental viscosity data, the Carreau–Yasuda model can describe the rheological behavior of the SWCNT/epoxy mixtures more accurately because it provides physically meaningful parameters associated with nanotube network breakdown and alignment under shear. In contrast, the Herschel–Bulkley model assumes the existence of a yield stress (σ_y). Therefore, the Carreau–Yasuda model offers a more physically appropriate description of the rheological behavior of the SWCNT/epoxy system.

Table 5. Summary of Herschel-Bulkley model parameters

Parameters	Concentration (wt%)			
	0.030	0.050	0.100	0.150
η_o	2.15	0.370	1.79	13.0
K	7.28	19.3	20.3	19.6
n	0.460	0.470	0.360	0.287
R^2	0.995	0.998	0.999	0.993

Optical microscopy images of the SWCNT/epoxy mixtures at different concentrations are shown in Figure 11. The 0.03 and 0.05 wt. % SWCNT epoxy mixtures show better dispersion states, whereas there are some aggregated clusters at higher concentrations.

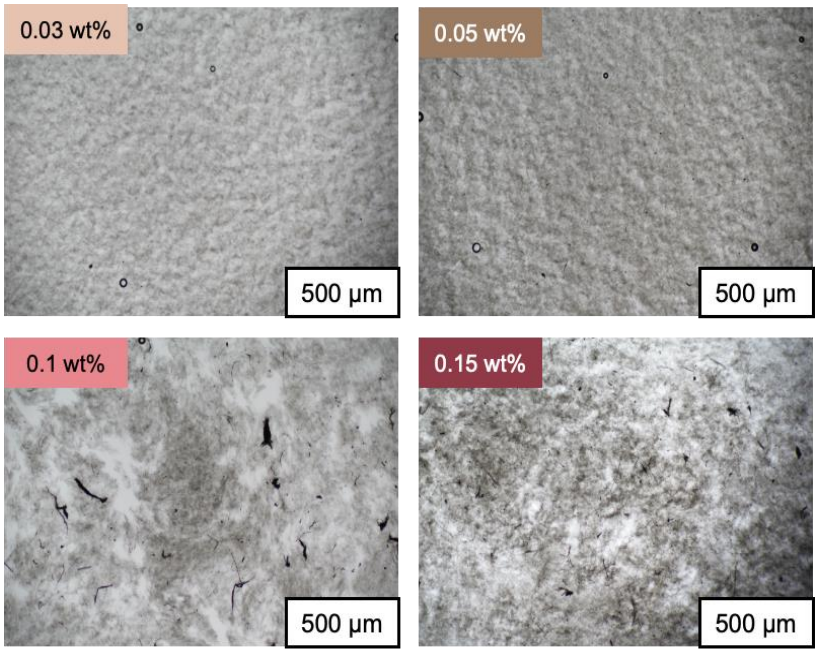

Figure 11. Optical microscopy images of the SWCNT/epoxy mixtures at different concentrations.

G'-G'' analysis of SWCNT-epoxy mixtures

Figure 12 shows the storage modulus (G') and loss modulus (G'') of different SWCNT-epoxy mixtures with varying concentrations versus strain. As mentioned in the background section, G' corresponds to the average stored energy per unit volume, whereas G'' reflects the average dissipated energy per unit volume during oscillatory shear. At low strain amplitudes, both G' and G'' of all mixtures remained constant, indicating the linear viscoelastic regime (LVR) (48, 61). The magnitudes of both G' and G'' increased with increasing SWCNT concentration, demonstrating that the incorporation of SWCNTs enhanced both the elastic and viscous responses of the nanocomposites. The highest moduli were observed for the 0.15 wt% mixture, suggesting restricted polymer chain mobility.

For all mixtures, G' was greater than G'' throughout the linear regime, indicating that the mixtures exhibited predominantly elastic or solid-like behavior. Beyond the G'-G'' crossover point, G' drops more rapidly than G'', indicating a nonlinear viscoelastic regime. The G'-G'' crossover point is often referred to as the flow point. Beyond this point, G'' was greater than G,' indicating that the dissipated energy dominated the stored energy (48, 62). According to Figure 11, at higher SWCNT concentrations, such as 0.15 wt%, the crossover point is pushed to a higher strain, suggesting that samples with higher nanotube loadings possess greater resistance to deformation.

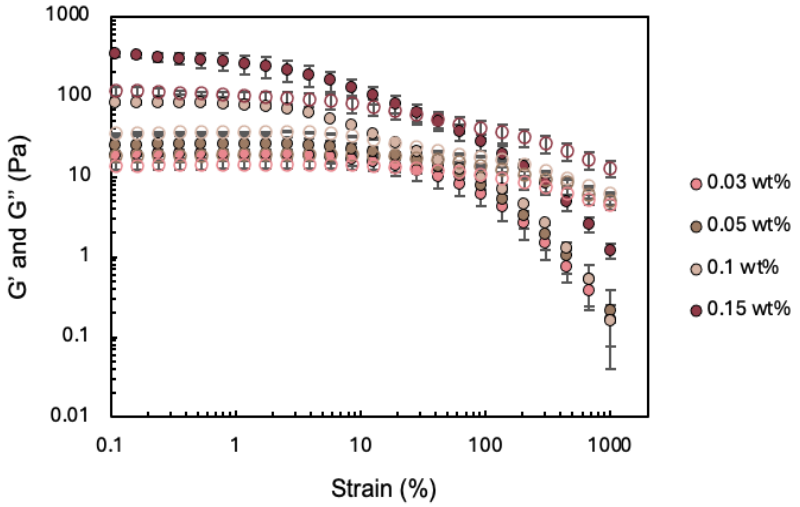

Figure 12. G' and G'' of mixtures vs. strain.

FT-Rheology of SWCNT-epoxy mixtures

FT rheology has been widely applied to investigate the nonlinear rheological behavior of complex fluids. Figure 13 shows the relative third harmonic $I_{3/1}$ as a function of the strain amplitude at a frequency of 0.8 rad/s. In the linear viscoelastic regime, the relative third harmonic reflects to nonlinearities due to instrumentation noise. In the medium-amplitude oscillatory shear (MAOS) regime, which is between SAOS and

LAOS, the relative third harmonic $I_{3/1}$ can be used to study the onset of nonlinearities in mixtures (48, 63).

According to Figure 13, the increase in the SWCNT concentration increases the $I_{3/1}$ of mixtures in the MAOS regime. The jump between the relative third harmonics of 0.05 and 0.1 wt% indicates the presence of a percolated network between these two concentrations. This supports the power law analysis findings. At 0.1 wt%, whereas above the percolation, the deformation of the interconnected SWCNT network generates much stronger nonlinearities, leading to larger third-harmonic intensities (49, 63). Furthermore, increasing the concentration of SWCNTs decreases the slope of $I_{3/1}$ in the MAOS regime.

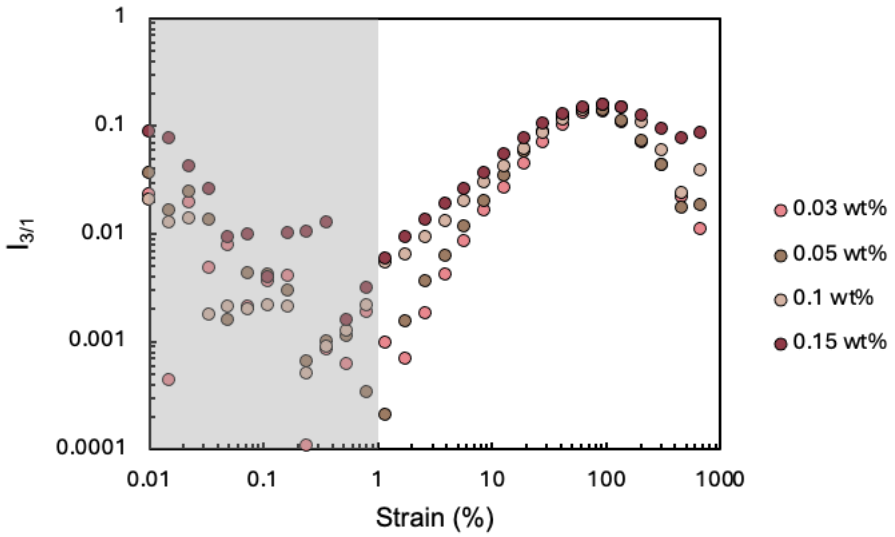

Figure 13. FT-rheology results for different SWCNT/epoxy mixtures; the grey box shows the out-of-torque data.

Lissajous-Bowditch (L-B) plots of SWCNT-epoxy mixtures

Lissajous plots can be used to investigate the viscoelastic behavior of complex fluids and mixtures. The L-B curves can show an elastic perspective, where stress is

plotted versus strain, and a viscous perspective, where stress is plotted versus shear rate. For viscoelastic materials, the L-B plots in the linear regime are elliptical. As the material response deviates from the linear viscoelastic regime, higher harmonic contributions become increasingly significant in the shear stress waveform, indicating nonlinear viscoelastic behavior (64, 65).

Figure 14 shows the elastic perspective of SWCNT-epoxy mixtures with 0.03 and 0.15 wt% SWCNTs at strains of 205%, 454%, 676%, and 1000%. As can be seen from the elastic perspective of 0.15 wt% SWCNTs at a strain of 205%, the transition from an ellipsoidal shape is more noticeable than that of the 0.03 wt% SWCNT epoxy mixture. In the L-B plots, the area enclosed by the curve represents the energy dissipated during a single oscillatory cycle and serves as an indicator of the viscous energy losses of the material (47, 65). Based on Figure 14, the area of the elastic perspective of 0.15 wt% at all strains is larger than that of 0.03 wt%, suggesting that increasing the SWCNT concentration increases the energy dissipation in the system. Moreover, the shape of the elastic perspective for 0.15 wt% at a strain of 1000% is more rectangular than that for 0.03 wt%, which shows that the mixture is more elastic at this concentration (66).

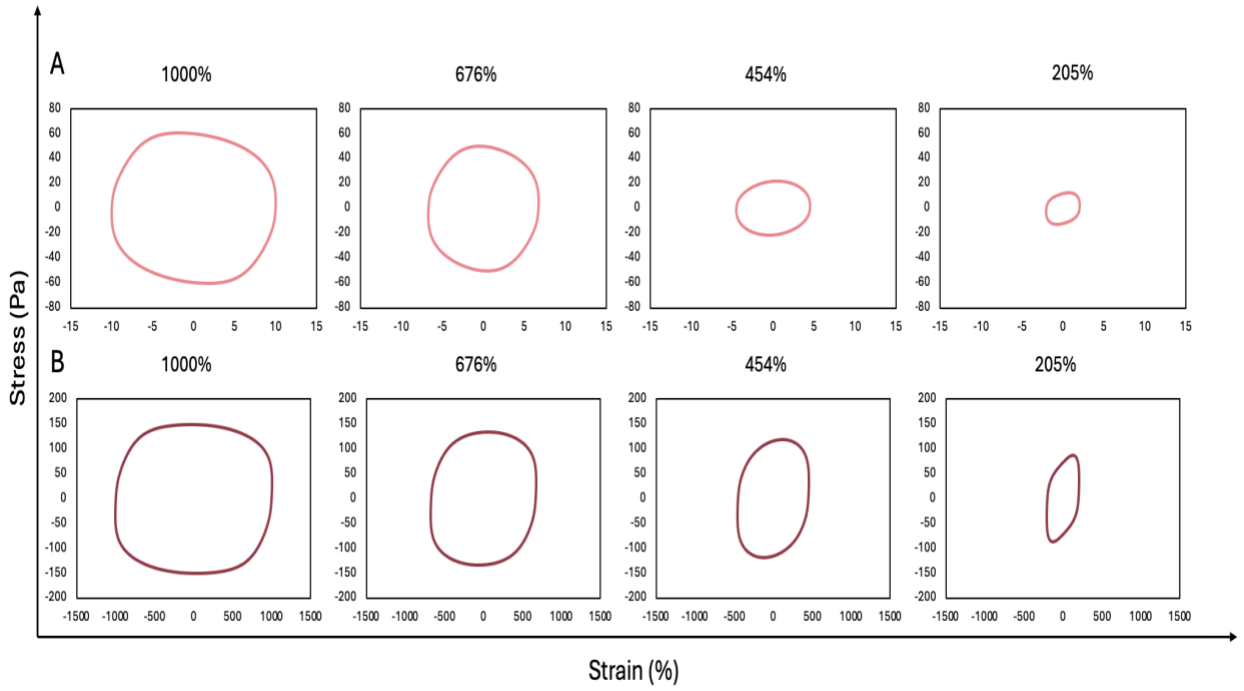

Figure 14. Elastic perspective of L-B plots for (A) 0.03 wt% SWCNTs and (B) 0.15 wt% SWCNT epoxy mixtures.

Figure 15 presents the viscous Lissajous–Bowditch curves of the SWCNT/epoxy mixtures containing 0.03 and 0.15 wt% SWCNTs. At 0.03 wt%, the enclosed area remained relatively narrow, even at high strain amplitudes, indicating limited energy dissipation during each oscillatory cycle. In contrast, the 0.15 wt% sample exhibited a substantially larger enclosed area, reflecting increased viscous energy dissipation and a stronger nonlinear response. As the strain amplitude reached 1000%, the viscous curve of the 0.15 wt% nanocomposite developed a sigmoidal shape, which is characteristic of strong shear-thinning behavior and significant microstructural rearrangement under deformation. Furthermore, self-intersections were observed at high strain amplitudes in the 0.03 wt% sample. These features may be attributed to the rapid microstructural reorganization occurring on timescales shorter than the applied oscillatory deformation,

resulting in a delayed stress response and complex nonlinear behavior. Overall, the differences between the two concentrations suggest that increasing the SWCNT content enhances network formation and promotes greater energy dissipation through nonlinear structural dynamics (66, 67).

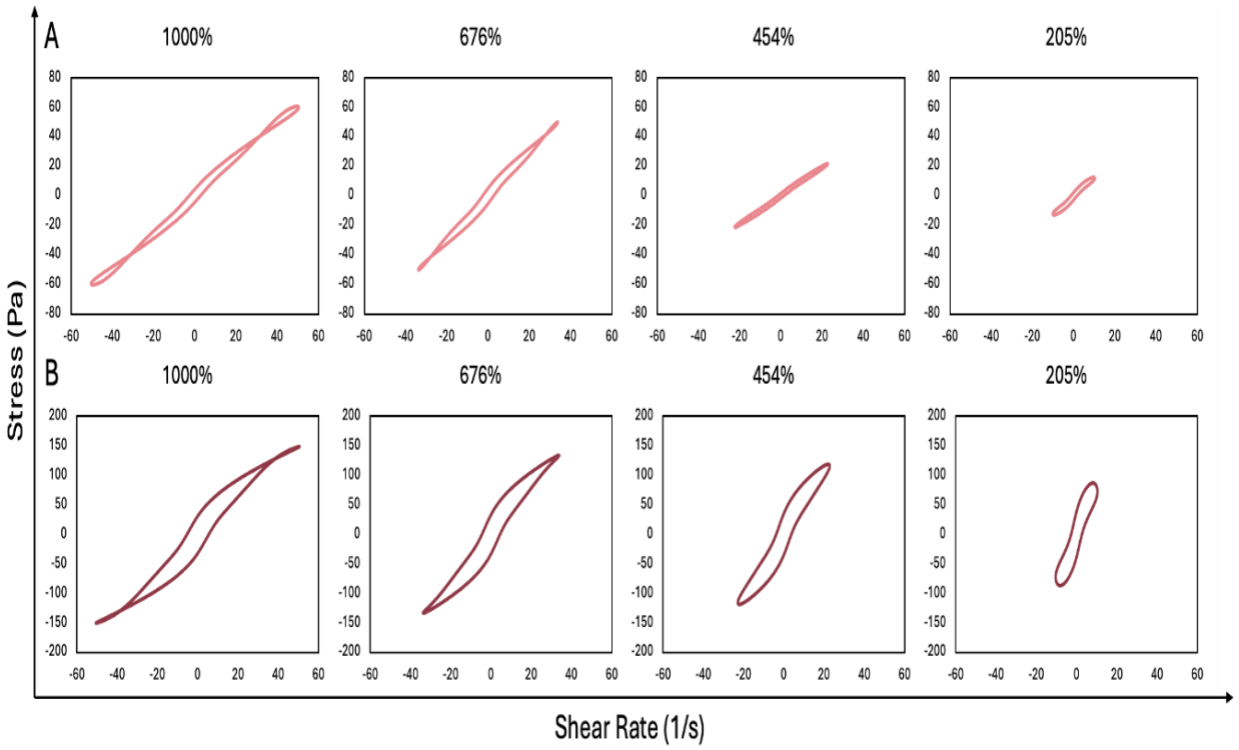

Figure 15. Viscous perspective of L-B plots for (A) 0.03 wt% SWCNTs and (B) 0.15 wt% SWCNT epoxy mixtures.

The ratio of S and T of SWCNT-epoxy mixtures

In the LAOS regime, where the L-B plots deviate from ellipses, the stress-strain relation cannot be described by linear differential equations with constant coefficients. This distortion of the response is usually because the modulus and viscosity depend on time within the oscillation. To record the intra-cycle variations, the local moduli and viscosities are defined as follows:

$$G'_M \equiv \left.\frac{d\sigma}{d\dot{\gamma}}\right|_{\gamma=0} \quad (7)$$

$$G'_L \equiv \left.\frac{\sigma}{\gamma}\right|_{\gamma=\pm\gamma_0} \quad (8)$$

$$\eta'_M \equiv \left.\frac{d\sigma}{d\dot{\gamma}}\right|_{\dot{\gamma}=0} \quad (9)$$

$$\eta'_L \equiv \left.\frac{\sigma}{\dot{\gamma}}\right|_{\dot{\gamma}=\pm\dot{\gamma}_0} \quad (10)$$

Where G'_M is the minimum-strain modulus, G'_L is the large-strain modulus, η'_M is the minimum-rate viscosity, and G'_L is the large-rate viscosity. Based on these definitions, the intracycle nonlinearity parameter S and T ratios are defined as

$$S \equiv \frac{G'_L - G'_M}{G'_L} \quad (11)$$

$$T \equiv \frac{\eta'_L - \eta'_M}{\eta'_L} \quad (12)$$

Where S is the strain-stiffening ratio and T is the shear-thickening ratio (48, 65, 68).

S > 0 implies intracycle strain stiffening, and S < 0 implies intracycle strain softening. A negative value of T refers to shear thinning, whereas a positive value of T refers to shear thickening. In the SAOS regime, both S and T were close to zero for all mixtures, consistent with linear viscoelastic behavior (65, 68). According to Figure 16, all the mixtures exhibited shear thinning and strain stiffening at high strains. The shear-thinning behavior of the SWCNT-epoxy mixtures could be due to the collapse of the nanofiller network structures at high strains and the orientation of the SWCNTs. Increasing the SWCNT content increased the shear-thinning behavior of the mixtures.

The positive S values suggest that the SWCNT/epoxy mixtures exhibit strain-stiffening behavior, where the elastic resistance increases with strain due to nanotube alignment and load transfer within the network. At the highest SWCNT concentration

(0.15 wt%), the strain-stiffening ratio decreased, which may indicate that an interconnected nanotube network was already established at low strains, reducing the extent of further stiffening during deformation (65, 68).

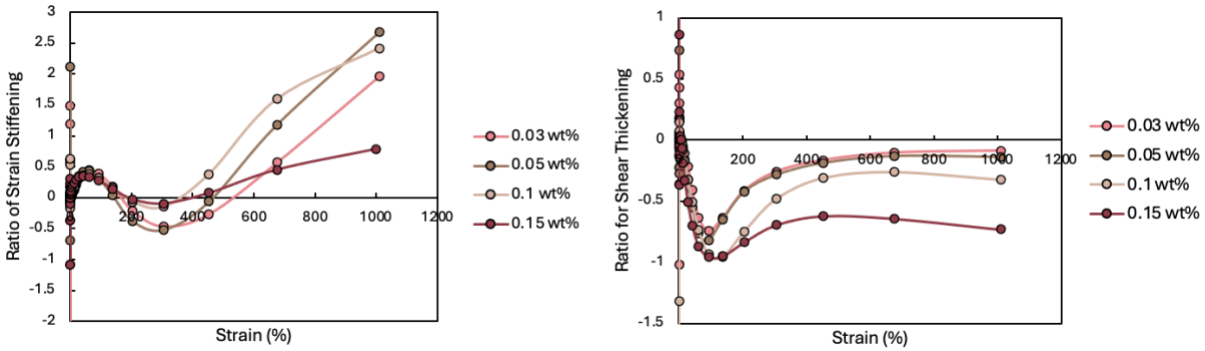

Figure 16. Ratio of strain stiffening and shear thickening of SWCNT/epoxy mixtures.

Raman mapping of nanocomposites

Figure 17 presents the Raman mapping images of the SWCNT/epoxy nanocomposites containing aligned and non-aligned SWCNTs at various concentrations. The maps were generated using the spatial intensity distribution of the G-band, which originates from the in-plane vibration of sp^2-hybridized carbon atoms in the SWCNT structure. Regions shown in yellow correspond to higher G-band intensities, indicating a greater local concentration of SWCNTs, whereas blue and purple regions represent lower intensities. The intensity of the G-band is highly dependent on the orientation of the nanotubes relative to the polarization direction of the incident laser due to the anisotropic nature of Raman scattering in carbon nanotubes. Consequently, regions containing SWCNTs aligned parallel to the laser polarization typically exhibit higher Raman intensities, whereas randomly oriented nanotubes produce a more heterogeneous intensity distribution. Therefore, variations in the G-

band intensity across the mapped area can be used to assess the spatial arrangement and degree of alignment of the SWCNTs within the epoxy matrix (69, 70).

Distinct vertically oriented stripe patterns were observed in the aligned nanocomposites, suggesting the preferential alignment of SWCNTs within the epoxy matrix. In contrast, the non-aligned samples exhibited more irregular and randomly distributed intensity patterns, consistent with random nanotube orientation. These results provide visual evidence of SWCNT alignment and demonstrate the effectiveness of the alignment process in inducing an anisotropic nanotube organization throughout the composite.

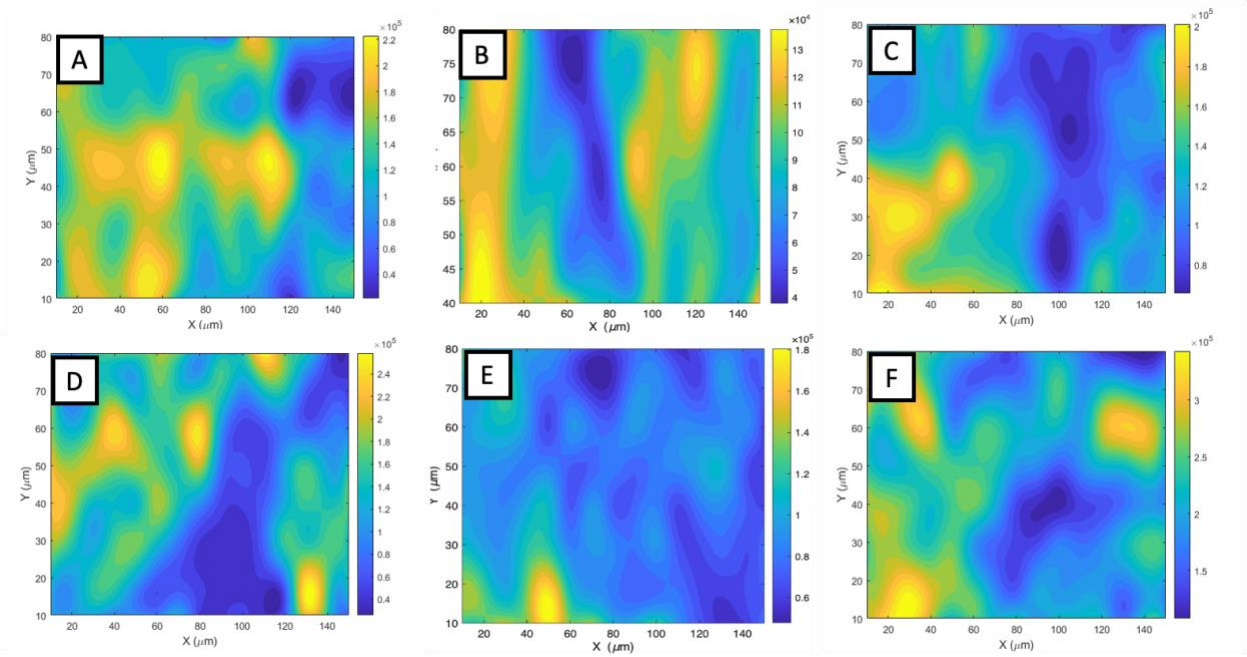

Figure 17. Raman maps of SWCNT-epoxy nanocomposites of aligned SWCNTs at concentrations of A) 0.03 wt%, B) 0.05 wt%, C) 0.07 wt%, and non-aligned SWCNTs at concentrations of D) 0.03 wt%, E) 0.05 wt%, and F) 0.07 wt%. Warmer colors (yellow) represent higher G-band intensities, while cooler colors (blue and purple) correspond to lower intensities. The strip-like high-intensity regions indicate alignment of SWCNTs within the epoxy matrix.

SEM results of nanocomposites

Figure 18 shows the SEM images of the fracture surfaces of the random and aligned SWCNT/epoxy nanocomposites containing 0.03, 0.05, and 0.07 wt% SWCNTs. While this provides only quantitative results on a small sample, some difference could be seen in Figure 18. For the random nanocomposites, distinct parallel features were clearly visible in the 0.07 wt% sample (Figure 18I), indicating an increase in the fracture surface roughness with increasing SWCNT concentration. This behavior suggests an enhanced resistance to crack propagation due to the higher SWCNT content (18, 71). In contrast, the random nanocomposites with lower SWCNT concentrations (0.03 and 0.05 wt%) exhibited relatively rough fracture surfaces but lacked well-defined parallel features. At a higher magnification (1 μm), CNT pull-out was observed in all random samples, indicating effective interfacial bonding between the SWCNTs and epoxy matrix that was sufficient to facilitate load transfer while still allowing nanotube pull-out. However, agglomerates or SWCNT bundles were also observed in the 0.07 wt% sample, suggesting regions of poor dispersion and weaker interfacial interactions between the epoxy matrix and SWCNTs, which could affect the mechanical performance of the nanocomposite (18, 72).

For the aligned nanocomposites, rounded parallel features were observed in samples 17D, H, and L, indicating a greater resistance to crack propagation, even at relatively low SWCNT loadings. These features suggest a change in the fracture mechanism resulting from the SWCNT alignment, which increases the crack path and promotes more energy-intensive fracture processes. CNT pull-out, visible as filament-

like structures emerging from the fracture surface, was observed in all the aligned samples, along with evidence of crack deflection. Although crack deflection was not apparent in the high-magnification images of the random nanocomposites, it was consistently observed in the aligned samples (Figure 18D, H and L), indicating an enhanced resistance to crack growth and failure. The combined presence of CNT pull-out and crack deflection suggests more effective stress transfer and toughening mechanisms in the aligned nanocomposites than in the random orientation (72-74).

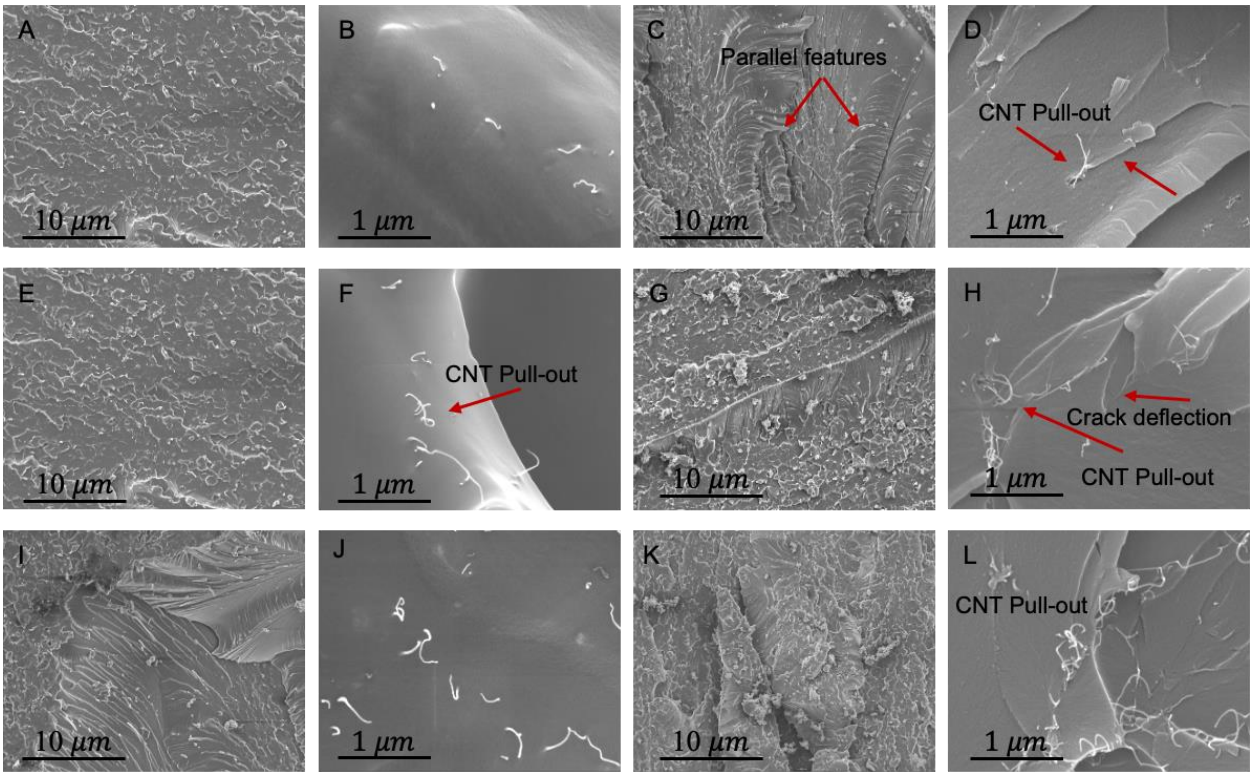

Figure 18. SEM images of (A), (B) 0.03 wt% random, (C), (D) 0.03 wt% aligned, (E), (F) 0.05 wt% random, (G), (H) 0.05 wt% aligned, (I), (J) 0.07 wt% random, (K), (L) 0.07 wt% aligned SWCNTs epoxy nanocomposites.

Curing rheology of SWCNT-epoxy mixtures

Figure 19 illustrates the evolution of the storage modulus (G′) and loss modulus (G″) during curing at 120 °C for mixtures containing different SWCNT concentrations. Three distinct stages can be identified throughout the curing process (75). In the initial stage, both G′ and G″ increase gradually as the epoxy system begins to polymerize and the primary network structure develops. During the second stage, a rapid increase in both moduli is observed, corresponding to extensive crosslinking and the formation of a continuous three-dimensional network. This sharp rise in viscoelastic properties reflects the transition from a liquid-like system to a gelled structure with increasing elasticity. In the final stage, G′ and G″ approach a plateau, indicating that the curing reaction is nearing completion and the network structure has become fully established.

The highest crossover point between G′ and G″ was taken as the gel time. The gel time of 0.03, 0.05, and 0.07 wt% is 105, 70, and 53 minutes, respectively. As shown in Figure 18, the gel time decreases with increasing SWCNT concentration, suggesting that the presence of SWCNTs accelerates network formation during the curing process (75, 76). Furthermore, the nanotube network may restrict polymer chain mobility and contribute to the earlier development of an interconnected structure within the curing system.

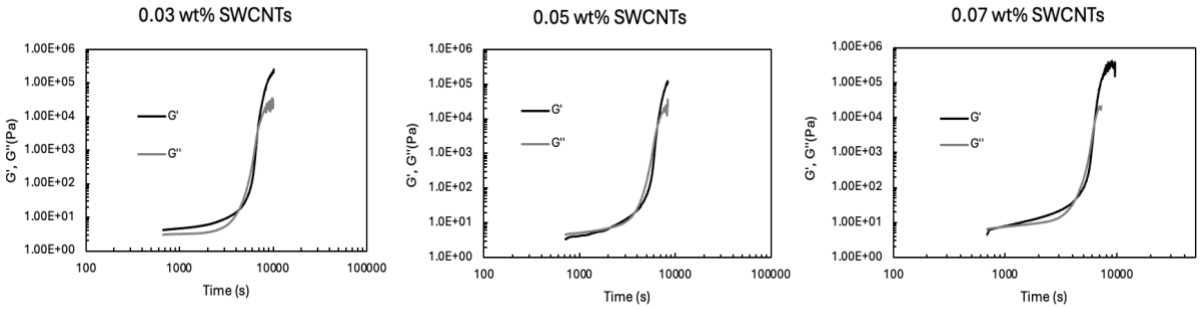

Figure 19. Time evolution of G’ and G’’ during curing process at 120 °C.

Mechanical properties of SWCNT-epoxy nanocomposites

Figure 20 presents the mechanical properties of the random and aligned SWCNT epoxy nanocomposites containing different SWCNT loadings (This part of research has done by Dr. Julkarnyne M Habibur Rahman and Dr. Gururaja group). As shown in Figure 19(A) and (B), the tensile strength of the randomly dispersed composites increased with increasing SWCNT concentration to 0.05 wt%. Specifically, the tensile strength increased by approximately 3.6% and 22.5% for the 0.03 wt% and 0.05 wt% samples, respectively, compared to that of the neat epoxy. However, a further increase in the SWCNT concentration to 0.07 wt% resulted in a 23% reduction in the tensile strength relative to that of the 0.05 wt% sample. This behavior suggests that the rheological percolation threshold occurs near 0.05 wt%, which is consistent with the rheological results. Beyond this concentration, increased nanotube–nanotube interactions and van der Waals attractions promote agglomeration, which adversely affects the stress transfer efficiency and consequently reduces the mechanical performance of the composites (77, 78).

The aligned SWCNT-epoxy nanocomposites (the alignment was performed along the longitudinal direction of the tensile bars) exhibited significantly higher tensile strength than their randomly dispersed counterparts. At 0.05 wt%, alignment resulted in an improvement of approximately 37% compared to the 22.5% increase observed for the random sample. More importantly, the alignment process effectively lowers the percolation threshold. The 0.03 wt% composite with randomly dispersed CNTs exhibited only a 3.6% increase in tensile strength compared to the neat epoxy. However, when the CNTs were aligned, the tensile strength increased by nearly 90% relative to the

corresponding randomly dispersed composite. Furthermore, after alignment, the difference in tensile strength between the 0.03 wt% and 0.05 wt% nanocomposites was reduced to approximately 2%, whereas it was approximately 83% before alignment. These results indicate that the preferential nanotube orientation along the loading direction enhances the reinforcement efficiency and lowers the effective percolation threshold. This improvement was attributed to the stronger nanotube interactions by the AC electric field, which facilitated a more efficient load transfer between the SWCNTs and epoxy matrix (17, 77).

The tensile modulus results shown in Figure 19(C) and (D) follow a similar trend. The aligned composites exhibited greater stiffness than the corresponding random composites, reflecting improved load transfer through the oriented nanotube network. In contrast, the modulus of the random 0.07 wt% sample decreased, further supporting nanotube aggregation at higher concentrations. Interestingly, at 0.03 wt%, the modulus enhancement was lower in the aligned samples than that in the random samples. This behavior may be attributed to the relatively low SWCNT concentration, which is insufficient to form a continuous stress-transfer network in the small-strain regime, despite nanotube alignment. Conversely, randomly dispersed nanotubes can form localized percolated structures that contribute more effectively to the initial elastic response.

At the lowest SWCNT loading (0.03 wt%), the increase in the tensile strength was accompanied by a smaller increase in the tensile modulus. This seemingly contradictory behavior can be explained by the strong interfacial bonding between the

SWCNTs and epoxy matrix. Efficient interfacial load transfer can significantly improve the tensile strength while having a less pronounced effect on the modulus, which is governed primarily by the material response at small strains. Additionally, the nanotube geometry, particularly the diameter and effective volume fraction, may further influence the relative improvements in strength and stiffness (18).

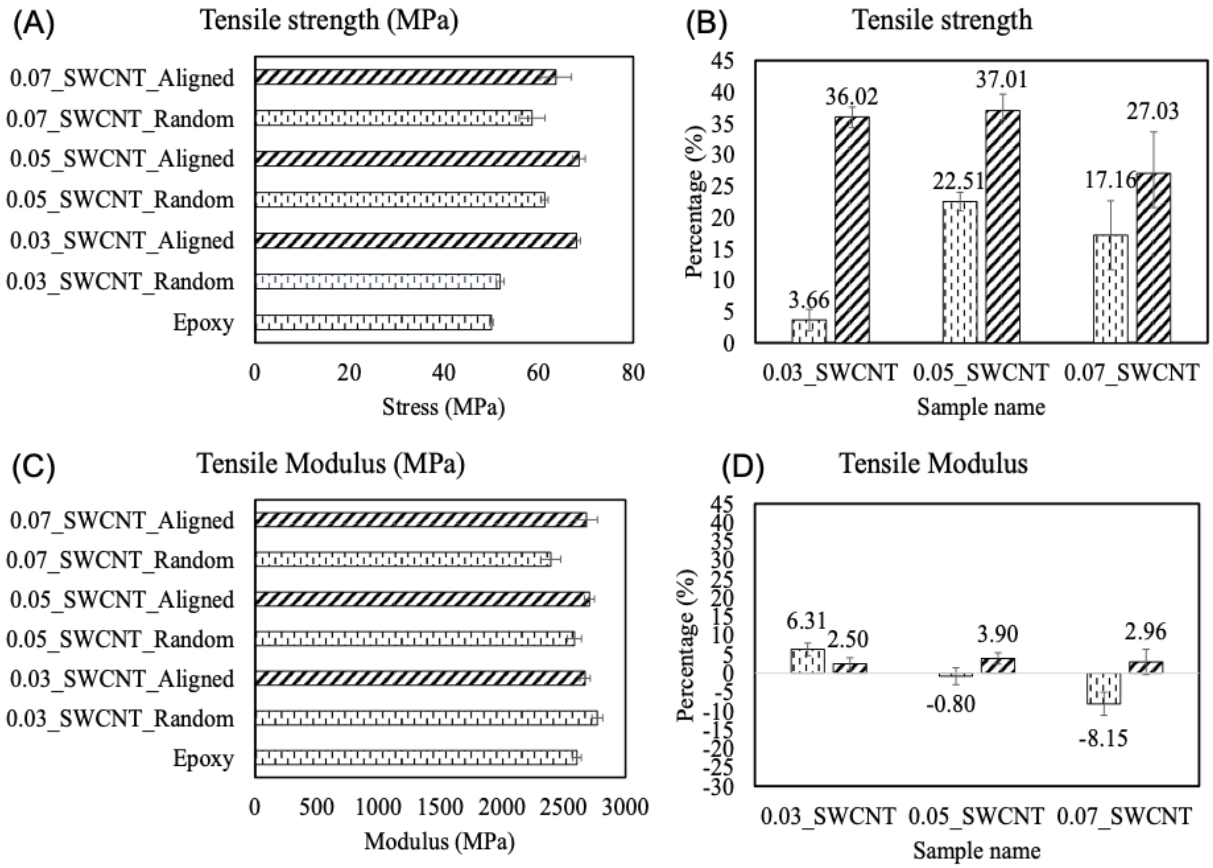

Figure 20. Mechanical properties of SWCNT Epoxy nanocomposites (a) tensile strength properties, (b) percentage enhancement in tensile strength, (c) tensile modulus properties, and (d) percentage enhancement in tensile modulus. This part of research was conducted by Dr. Julkarnyne M Habibur Rahman and Dr. Gururaja group.

Linear rheology of SWCNT-GO epoxy mixture

Numerous studies have investigated the synergistic effects of combining CNTs with graphene oxide (GO) sheets, as GO can help reduce the agglomeration of CNTs and promote a more uniform dispersion within the epoxy matrix. In addition, the oxygen-containing functional groups on GO improve its compatibility and interfacial interactions with the epoxy resin (31). Figure 21 presents the storage modulus (G') and loss modulus (G'') as a function of angular frequency for the SWCNT-GO epoxy mixtures prepared using methods A and B. For both preparation methods, the SWCNT-GO mixtures with a 1:1 ratio exhibited substantially higher G' and G'' values than the corresponding 1:3 mixtures across the entire frequency range, indicating the formation of a stronger and more interconnected filler network.

A crossover point, where G' and G'' are equal in magnitude, was observed for all mixtures. Below the crossover frequency, the elastic response dominates the viscoelastic behavior, whereas above the crossover frequency, the viscous response becomes increasingly significant (1). As shown in Figure 21, the crossover frequency shifted to higher values for the B-1:1 and B-1:3 mixtures compared with their counterparts prepared using method A. This behavior suggests that the networks formed by method B remain elastic-dominant over a broader frequency range, indicating enhanced network stability and stronger filler-filler interactions. The shift in crossover frequency could also reflect improved filler dispersion and more effective network formation achieved through method B (57).

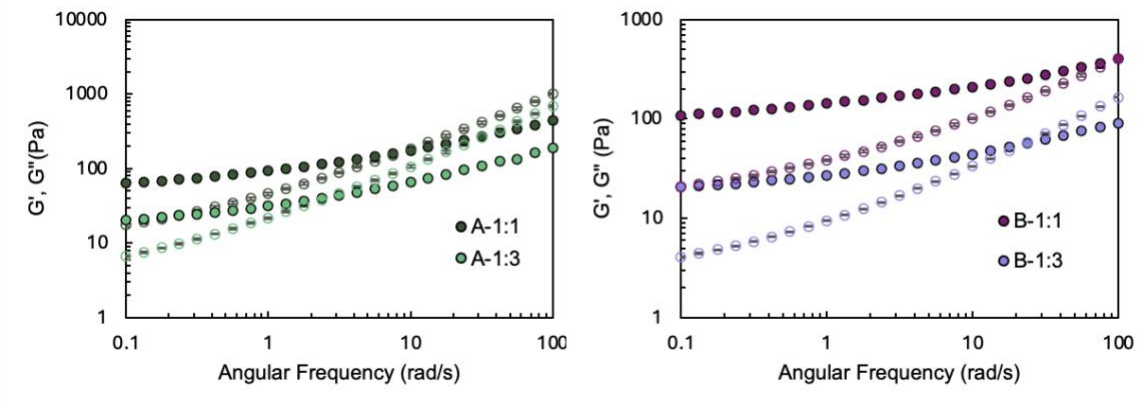

Figure 21. Frequency sweep of 0.2 wt% SWCNT-GO epoxy mixtures.

Microscopy images of the SWCNT-GO epoxy mixtures are shown in Figure 22. Some aggregated clusters can be seen in both SWCNT-GO epoxy mixtures with a ratio of 1:1, which suggests that mixtures with a ratio of 1:1 likely are above percolation. Furthermore, a better dispersion state was observed in the mixtures prepared using method B than in those prepared using method A.

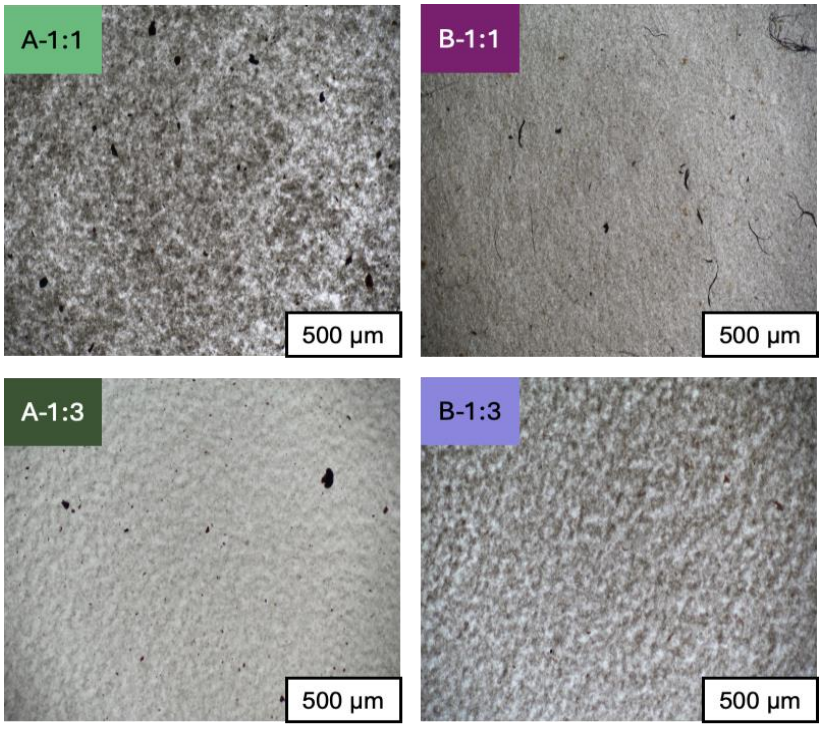

Figure 22. Optical microscopy images of different 0.2 wt% SWCNT-GO epoxy mixtures.

The G'-G'' analysis and FT-Rheology of SWCNT-GO epoxy mixtures

The storage modulus (G') of the SWCNT-GO epoxy mixtures as a function of strain and FT-rheology results are displayed in Figure 23. The SWCNT-GO epoxy mixtures with a ratio 1:1 have a higher storage modulus than mixtures with a ratio 1:3, suggesting a stronger network connection in these mixtures. While the amplitude sweep results could provide valuable information about the difference between two different ratios of SWCNT-GO epoxy mixtures, it suggests that there is not much difference in the dispersing methods or the aggregation state that was obtained.

As mentioned before, the slope of the $I_{3/1}$ versus strain in the MAOS regime can provide valuable information on the nonlinearities of the mixtures (79). According to Figure 23, the B-1:3 mixture has a lower relative third harmonic than the other SWCNT-GO epoxy mixtures. This could be due to the weak nonlinear behavior of this mixture compared to the others (63). Furthermore, while the A-1:1 and B-1:1 mixtures have almost the same relative third harmonic, B-1:3 has a higher $I_{3/1}$ than the other mixtures. This could be attributed to the better dispersion state and less aggregated network in this mixture (80). It should be noted that while the storage modulus versus strain did not show any distinction between the mixtures made using the two different methods, FT-rheology showed a distinction between them.

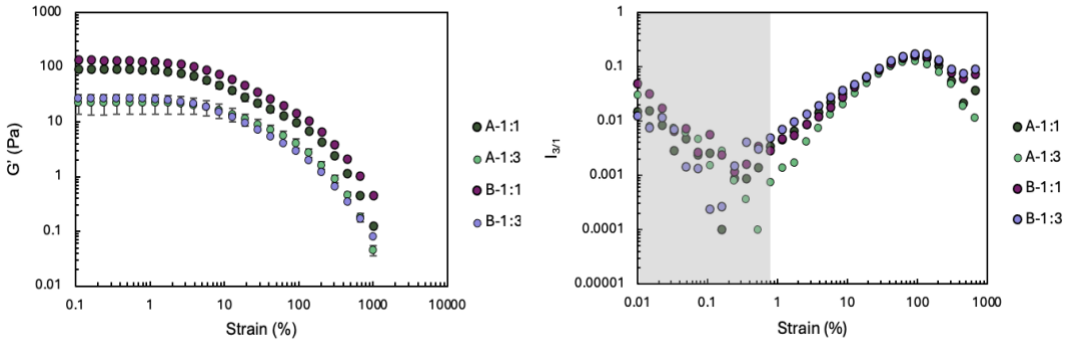

Figure 23. Amplitude sweep and FT-rheology of 0.2 wt% SWCNT-GO epoxy mixtures; the grey box shows the out-of-torque data.

Lissajous-Bowditch (L-B) plots of SWCNT-GO epoxy mixtures

The elastic perspective of the SWCNT-GO epoxy mixtures at a strain of 1000% is highlighted in Figure 24. As mentioned previously, deviations from the elliptical form reflect the onset of the nonlinear behavior of the mixtures. The elastic perspective curves of the SWCNT-GO epoxy mixtures made using method B were more rectangular with rounded corners than those of the mixtures made using method A. This could be attributed to a better plastic yield stress response in mixtures made with method B (67).

The enclosed area of the SWCNT-GO epoxy mixture with a 1:1 ratio was larger than that of the mixture with a 1:3 ratio. The larger enclosed area observed in the elastic Lissajous–Bowditch curves of the SWCNT–GO epoxy nanocomposites with a 1:1 ratio indicates greater energy dissipation during each oscillatory cycle compared to the 1:3 system. This behavior could be associated with the formation of a more interconnected hybrid filler network in which the SWCNTs effectively bridge adjacent GO sheets and enhance the interparticle interactions. The resulting network undergoes structural

rearrangement and bond disruption under deformation, leading to increased viscous energy losses (64, 66).

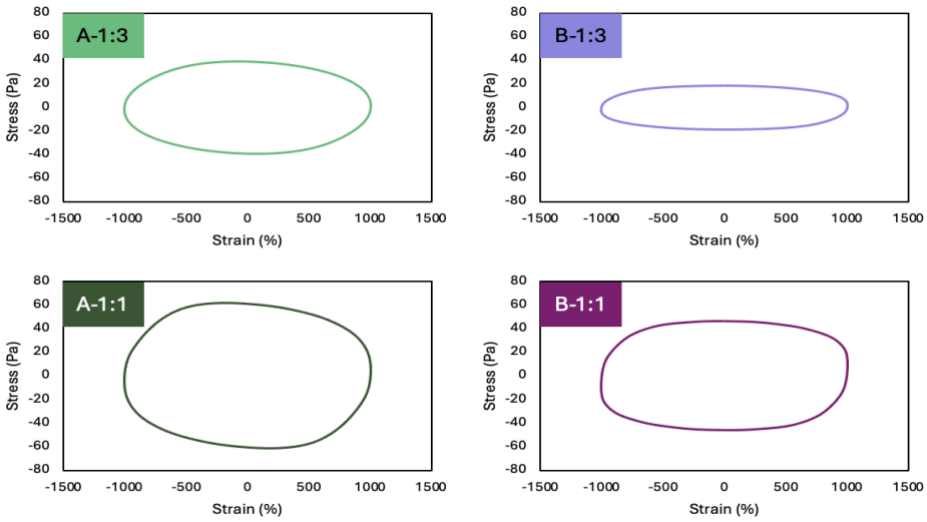

Figure 24. Elastic perspectives of 0.2 wt% SWCNT-GO epoxy mixtures at a strain of 1000%.

Figure 25 displays the viscous L-B perspective curves of the SWCNT-GO epoxy mixtures with ratios of 1:3 and 1:1. The 1:3 mixtures exhibited relatively narrow and nearly linear loops, indicating limited viscous energy dissipation and weaker nonlinear behavior. In contrast, the mixtures with a ratio of 1:1 displayed substantially larger enclosed areas and pronounced sigmoidal distortions, reflecting increased energy dissipation during each oscillatory cycle (49, 66). The larger loop areas suggest that SWCNT-GO with a ratio of 1:1 undergoes more extensive microstructural rearrangement and exhibits stronger nonlinear viscoelastic behavior. This response was attributed to the formation of a more interconnected hybrid filler network in which the SWCNTs effectively bridged the GO sheets and enhanced the filler-filler interactions. These results indicate that the 1:1 ratio provides more effective network formation and

stronger synergistic interactions between SWCNTs and GO than the SWCNT-GO epoxy mixtures (1:3).

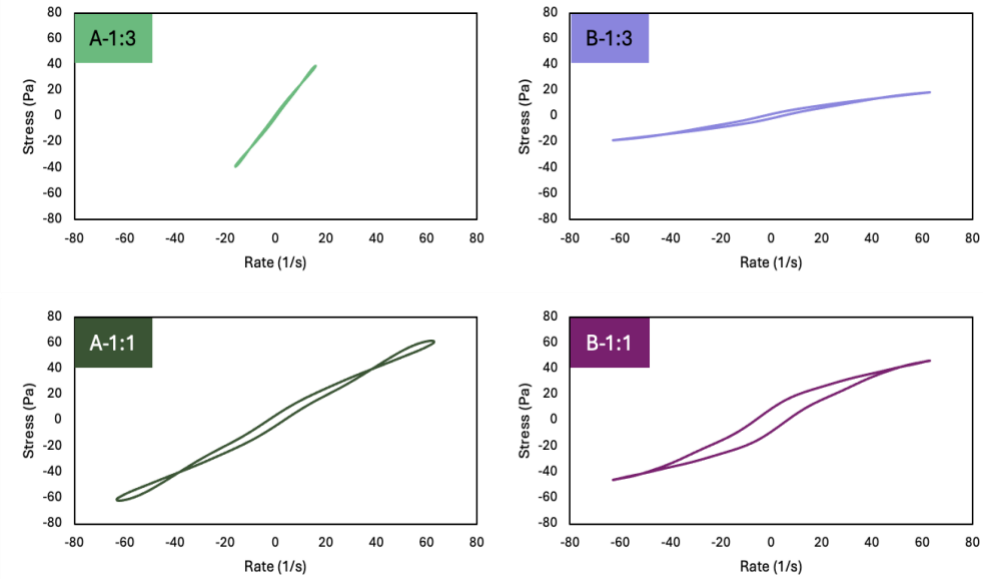

Figure 25. Viscous perspectives of 0.2 wt% SWCNT-GO epoxy mixtures at a strain of 1000%.

The ratio of S and T of SWCNT-GO epoxy mixtures

Figure 27 shows the strain-stiffening ratio (S) and shear-thickening ratio (T) of the SWCNT–GO epoxy mixtures. All the mixtures exhibited shear-thinning ($T < 0$) and strain-stiffening ($S > 0$) behaviors**.** The A-1:1 and A-1:3 mixtures showed similar values of S and T, suggesting that the SWCNT-to-GO ratio has a limited effect on the nonlinear rheological response when Method A is used.

In contrast, the mixtures prepared using Method B exhibited more shear thinning and lower strain stiffening than those prepared using Method A. The enhanced shear-thinning behavior may be attributed to the improved dispersion of the nanofillers, which promotes nanotube alignment and network rearrangement under deformation. The

reduction in strain stiffening suggests that the nanofiller network was more uniformly distributed and well developed at low strains, resulting in less additional stiffening during large-amplitude deformation. These results indicate that Method B produces stronger nanofiller–matrix interactions within the epoxy system (65, 68, 81).

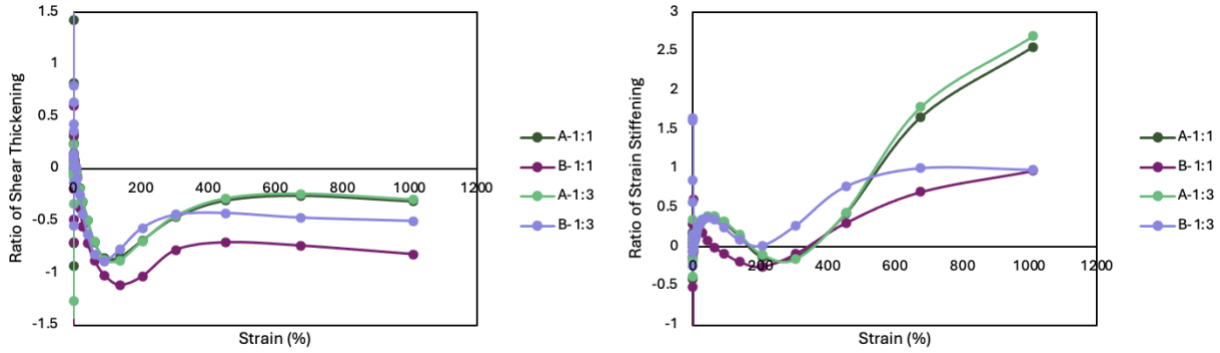

Figure 26. Ratio of strain stiffening and shear thickening of 0.2 wt% SWCNT-GO epoxy mixtures.

Chapter 5: Conclusion and Future Directions

This study aimed to provide further insight into the dispersion state of single-walled carbon nanotubes (SWCNTs) in epoxy resin using both linear and nonlinear rheological techniques. In the first part of this study, epoxy mixtures containing different concentrations of SWCNTs were prepared to evaluate the rheological percolation threshold of nanofillers within the polymer matrix. Both linear and nonlinear rheological analyses indicated that the critical concentration of SWCNTs in epoxy resin was approximately 0.05 wt%.

In the second part of the research, an electric field was applied to align the SWCNTs within the epoxy resin prior to the addition of the curing agent, allowing the influence of nanotube alignment on the curing behavior and rheological properties of the mixtures to be investigated. Scanning electron microscopy (SEM) and Raman mapping were employed to characterize the alignment process and confirm the orientation of the SWCNTs within the epoxy matrix. The results demonstrated that nanotube alignment reduced the mechanical percolation threshold to approximately 0.03 wt%, highlighting the significant influence of the filler orientation on network formation and microstructure development.

In the final part of this study, graphene oxide (GO) was introduced as a secondary nanofiller to investigate its effect on the dispersion state of SWCNTs and to

evaluate the potential synergistic interactions between the two nanomaterials. Two preparation methods and two SWCNT:GO ratios were examined to identify the conditions that promoted improved nanofiller dispersion. The results showed that dispersing GO in ethanol prior to mixing enhanced the dispersion quality of the SWCNT–GO epoxy system. Furthermore, the SWCNT:GO (1:3) mixture exhibited a more homogeneous dispersion than the SWCNT:GO (1:1) mixture.

Overall, the results demonstrate that while linear rheology can provide valuable information about the microstructures of mixtures, nonlinear rheology can be a more powerful method for assessing and distinguishing the dispersion state and microstructural evolution of nanofillers in epoxy systems. The findings further show that nanotube alignment and GO incorporation can significantly influence the rheological behavior and percolation characteristics of SWCNT-based epoxy nanocomposites.

Future studies should focus on applying additional nonlinear rheological techniques, such as the Sequence of Physical Processes (SPP) framework, to further investigate the nonlinear deformation mechanisms and microstructural evolution of CNT-based systems. These approaches can provide deeper insights into the structural rearrangements, network breakdown, and recovery processes that occur under large deformations.

In addition, the methodology developed in this study can be extended to other one-dimensional (1D) and two-dimensional (2D) nanomaterials, including carbon nanofibers, graphene nanoplatelets, and transition metal dichalcogenides. By combining linear and nonlinear rheological characterizations, future studies can establish relationships between nanofiller dispersion, network formation, and rheological behavior, leading to a better understanding of the microstructure–property relationships in advanced polymer nanocomposites.

Reference

1. Goswami J, Davis VA. Viscoelasticity of single-walled carbon nanotubes in unsaturated polyester resin: effects of purity and chirality distribution. Macromolecules. 2015;48(23):8641–50.
2. Rana S, Alagirusamy R, Joshi M. A review on carbon epoxy nanocomposites. Journal of Reinforced Plastics and Composites. 2009;28(4):461–87.
3. Singh NP, Gupta V, Singh AP. Graphene and carbon nanotube reinforced epoxy nanocomposites: A review. Polymer. 2019;180:121724.
4. Mittal V, Saini R, Sinha S. Natural fiber-mediated epoxy composites–a review. Composites Part B: Engineering. 2016;99:425–35.
5. Dong M, Zhang H, Tzounis L, Santagiuliana G, Bilotti E, Papageorgiou DG. Multifunctional epoxy nanocomposites reinforced by two-dimensional materials: A review. Carbon. 2021;185:57–81.
6. Upadhyay AK, Goyat M, Kumar A. A review on the effect of oxide nanoparticles, carbon nanotubes, and their hybrid structure on the toughening of epoxy nanocomposites. Journal of Materials Science. 2022;57(28):13202–32.
7. Iqbal A, Saeed A, Ul-Hamid A. A review featuring the fundamentals and advancements of polymer/CNT nanocomposite application in aerospace industry. Polymer Bulletin. 2021;78(1):539–57.
8. Davis VA. Rheological and curing properties of unsaturated polyester resin nanocomposites. Unsaturated Polyester Resins: Elsevier; 2019. p. 471–88.
9. Kayatin MJ, Davis VA. In situ polymerization functionalization of single-walled carbon nanotubes with polystyrene. Journal of Polymer Science Part A: Polymer Chemistry. 2013;51(17):3716–25.
10. Nilagiri Balasubramanian KB, Ramesh T. Role, effect, and influences of micro and nano-fillers on various properties of polymer matrix composites for microelectronics: a review. Polymers for Advanced Technologies. 2018;29(6):1568–85.
11. Song YS, Youn JR. Influence of dispersion states of carbon nanotubes on physical properties of epoxy nanocomposites. Carbon. 2005;43(7):1378–85.
12. Dyachkova TP, Khan YA, Burakova EA, Galunin EV, Shigabaeva GN, Stolbov DN, et al. Characteristics of epoxy composites containing carbon nanotubes/graphene mixtures. Polymers. 2023;15(6):1476.
13. Syduzzaman M, Saad MSI, Piam MF, Talukdar TA, Shobdo TT, Pritha NM. Carbon nanotubes: Structure, properties and applications in the aerospace industry. Results in Materials. 2025;25:100654.
14. Thi TBN, Ata S, Morimoto T, Yamada T, Okazaki T, Hata K. Tailoring the electrically conductive network of injection-molded polymer-carbon nanotube composite at low filler content. Materials Today: Proceedings. 2021;40:5–8.
15. Butt HA, Lomov SV, Akhatov IS, Abaimov SG. Self-diagnostic carbon nanocomposites manufactured from industrial epoxy masterbatches. Composite Structures. 2021;259:113244.
16. Bandaru PR. Electrical properties and applications of carbon nanotube structures. Journal of Nanoscience and Nanotechnology. 2007;7(4-5):1239–67.

17. Moaseri E, Moaseri N, Maghrebi M, Baniadam M. Alignment of multiwalled carbon nanotubes-reinforced epoxy by a novel shear assisted method in the presence of the electric field. Polymer Composites. 2023;44(9):5830–8.
18. Khan SU, Pothnis JR, Kim J-K. Effects of carbon nanotube alignment on electrical and mechanical properties of epoxy nanocomposites. Composites Part A: Applied Science and Manufacturing. 2013;49:26–34.
19. Gupta P, Rajput M, Singla N, Kumar V, Lahiri D. Electric field and current assisted alignment of CNT inside polymer matrix and its effects on electrical and mechanical properties. Polymer. 2016;89:119–27.
20. Pothnis JR, Gururaja S, Kalyanasundaram D. Development and characterization of electric field directed preferentially aligned CNT nanocomposites. Mechanics of Advanced Materials and Structures. 2019;26(1):35–41.
21. Pothnis JR, Kalyanasundaram D, Gururaja S. Enhancement of open hole tensile strength via alignment of carbon nanotubes infused in glass fiber-epoxy-CNT multi-scale composites. Composites Part A: Applied Science and Manufacturing. 2021;140:106155.
22. Pothnis JR, Kalyanasundaram D, Gururaja S. Controlled manipulation of CNTs in glass/epoxy composites with cut-outs using non-uniform electric field. Advanced Composite Materials. 2021;30(3):205–21.
23. Pothnis JR, Kalyanasundaram D, Gururaja S. Mitigation of notch sensitivity by controlled alignment of carbon nanotubes in epoxy using electric field application. Composites Part A: Applied Science and Manufacturing. 2021;149:106544.
24. Malkina O, Mahfuz H, Sorge K, Rondinone A, Chen J, More K, Reeves S, Rangari V. Magnetic alignment of SWCNTs decorated with Fe_3O_4 to enhance mechanical properties of SC-15 epoxy. AIP Advances. 2013;3(4).
25. Wu S, Ladani RB, Zhang J, Kinloch AJ, Zhao Z, Ma J, Zhang X, Mouritz AP, Ghorbani K, Wang CH. Epoxy nanocomposites containing magnetite-carbon nanofibers aligned using a weak magnetic field. Polymer. 2015;68:25–34.
26. Haibat J, Ceneviva S, Spencer MP, Kwok F, Trivedi S, Mohney SE, et al. Preliminary demonstration of energy-efficient fabrication of aligned CNT-polymer nanocomposites using magnetic fields. Composites Science and Technology. 2017;152:27–35.
27. Monti M, Natali M, Torre L, Kenny JM. The alignment of single walled carbon nanotubes in an epoxy resin by applying a DC electric field. Carbon. 2012;50(7):2453–64.
28. Amani AM, Hashemi SA, Mousavi SM, Abrishamifar SM, Vojood A. Electric field induced alignment of carbon nanotubes: methodology and outcomes. Carbon nanotubes-recent progress: IntechOpen; 2017.
29. Maheshkumar K, Krishnamurthy K, Sathishkumar P, Sahoo S, Uddin E, Pal S, Rajasekar, R. Research updates on graphene oxide-based polymeric nanocomposites. Polymer composites. 2014;35(12):2297–310.
30. Shah R, Kausar A, Muhammad B, Shah S. Progression from graphene and graphene oxide to high performance polymer-based nanocomposite: a review. Polymer-Plastics Technology and Engineering. 2015;54(2):173–83.
31. Jyoti J, Singh BP. A review on 3D graphene–carbon nanotube hybrid polymer nanocomposites. Journal of Materials Science. 2021;56(31):17411–56.
32. Wu J-K, Ye C-C, Liu T, An Q-F, Song Y-H, Lee K-R, Hung W-S, Gao C-J. Synergistic effects of CNT and GO on enhancing mechanical properties and separation performance of polyelectrolyte complex membranes. Materials & Design. 2017;119:38–46.

33. Charitos I, Georgousis G, Klonos PA, Kyritsis A, Mouzakis D, Raptis Y, Kontos A, Kontou E. The synergistic effect on the thermomechanical and electrical properties of carbonaceous hybrid polymer nanocomposites. Polymer Testing. 2021;95:107102.
34. Dresselhaus MS, Dresselhaus G, Eklund PC. Science of fullerenes and carbon nanotubes: their properties and applications: Elsevier; 1996.
35. Davis VA, Green MJ. Controlling and characterizing anisotropic nanomaterial dispersion. Nanotechnology Commercialization: Manufacturing Processes and Products. 2017:65–99.
36. Israelachvili JN. Intermolecular and surface forces: Academic press; 2011.
37. Macosko CW. Rheology principles. Measurements and applications. 1994.
38. Gómez-Navarro C, Meyer JC, Sundaram RS, Chuvilin A, Kurasch S, Burghard M, et al. Atomic structure of reduced graphene oxide. Nano letters. 2010;10(4):1144–8.
39. Hiew BYZ, Lee LY, Lee XJ, Thangalazhy-Gopakumar S, Gan S, Lim SS, et al. Review on synthesis of 3D graphene-based configurations and their adsorption performance for hazardous water pollutants. Process Safety and Environmental Protection. 2018;116:262–86.
40. Schafhaeutl C. L. On the combinations of carbon with silicon and iron, and other metals, forming the different species of cast iron, steel, and malleable iron. The London, Edinburgh, and Dublin Philosophical Magazine and Journal of Science. 1840;16(103):297–304.
41. Hummers Jr WS, Offeman RE. preparation of graphitic oxide. Journal of the american chemical society. 1958;80(6):1339.
42. Trikkaliotis DG, Christoforidis AK, Mitropoulos AC, Kyzas GZ. Graphene oxide synthesis, properties and characterization techniques: a comprehensive review. ChemEngineering. 2021;5(3):64.
43. Balguri PK, Samuel DH, Thumu U. A review on mechanical properties of epoxy nanocomposites. Materials Today: Proceedings. 2021;44:346–55.
44. Kamal A, Ashmawy M, S S, Algazzar AM, Elsheikh AH. Fabrication techniques of polymeric nanocomposites: A comprehensive review. Proceedings of the Institution of Mechanical Engineers, Part C: Journal of Mechanical Engineering Science. 2022;236(9):4843–61.
45. Moniruzzaman M, Winey KI. Polymer nanocomposites containing carbon nanotubes. Macromolecules. 2006;39(16):5194–205.
46. Basavegowda N, Baek K-H. Advances in functional biopolymer-based nanocomposites for active food packaging applications. Polymers. 2021;13(23):4198.
47. Hyun K, Wilhelm M, Klein CO, Cho KS, Nam JG, Ahn KH, et al. A review of nonlinear oscillatory shear tests: Analysis and application of large amplitude oscillatory shear (LAOS). Progress in polymer science. 2011;36(12):1697–753.
48. Shim YH. Understanding nonlinear rheology in anisotropic colloids: a review. Korea-Australia Rheology Journal. 2025;37(3):373–88.
49. Kamkar M, Salehiyan R, Goudoulas TB, Abbasi M, Saengow C, Erfanian E, et al. Large amplitude oscillatory shear flow: Microstructural assessment of polymeric systems. Progress in Polymer Science. 2022;132:101580.
50. Cho KS, Hyun K, Ahn KH, Lee SJ. A geometrical interpretation of large amplitude oscillatory shear response. Journal of Rheology. 2005;49(3):747–58.
51. Rogers SA. A sequence of physical processes determined and quantified in LAOS: An instantaneous local 2D/3D approach. Journal of Rheology. 2012;56(5):1129–51.

52. Rogers SA, Lettinga MP. A sequence of physical processes determined and quantified in large-amplitude oscillatory shear (LAOS): Application to theoretical nonlinear models. Journal of rheology. 2012;56(1):1–25.
53. Shim YH, Rogers SA. Understanding the yielding behavior of graphene oxide colloids via experimental strain decomposition. Physics of Fluids. 2023;35(6).
54. Saito R, Takeya T, Kimura T, Dresselhaus G, Dresselhaus M. Raman intensity of single-wall carbon nanotubes. Physical Review B. 1998;57(7):4145.
55. Kayatin M. Rheology, Structure, and Stability of Carbon Nanotube-Unsaturated Polyester Resin Dispersions 2008.
56. Ureña-Benavides EE, Kayatin MJ, Davis VA. Dispersion and rheology of multiwalled carbon nanotubes in unsaturated polyester resin. Macromolecules. 2013;46(4):1642–50.
57. Kayatin MJ, Davis VA. Viscoelasticity and shear stability of single-walled carbon nanotube/unsaturated polyester resin dispersions. Macromolecules. 2009;42(17):6624–32.
58. Wozniak M, Rylski A, Lason-Rydel M, Orczykowska M, Obraniak A, Siczek K. Some rheological properties of plastic greases by Carreau-Yasuda model. Tribology International. 2023;183:108372.
59. Coclite A, Coclite GM, De Tommasi D. Capsules rheology in Carreau–Yasuda fluids. Nanomaterials. 2020;10(11):2190.
60. Saasen A, Ytrehus J. Viscosity Models for Drilling Fluids—Herschel-Bulkley Parameters and Their Use. Energies 13 (20): 5271. 2020.
61. Yang W, Byun JJ, Yang J, Moissinac FP, Peng Y, Tontini G, et al. Freeze-assisted tape casting of vertically aligned MXene films for high rate performance supercapacitors. Energy & Environmental Materials. 2020;3(3):380–8.
62. Griebler JJ, Rogers SA. The nonlinear rheology of complex yield stress foods. Physics of Fluids. 2022;34(2).
63. Lim HT, Ahn KH, Hong JS, Hyun K. Nonlinear viscoelasticity of polymer nanocomposites under large amplitude oscillatory shear flow. Journal of Rheology. 2013;57(3):767–89.
64. Schreuders F, Sagis L, Bodnár I, Erni P, Boom R, Van Der Goot A. Small and large oscillatory shear properties of concentrated proteins. Food Hydrocolloids. 2021;110:106172.
65. Kamkar M, Sadeghi S, Arjmand M, Sundararaj U. Structural characterization of CVD custom-synthesized carbon nanotube/polymer nanocomposites in large-amplitude oscillatory shear (LAOS) mode: Effect of dispersion characteristics in confined geometries. Macromolecules. 2019;52(4):1489–504.
66. Ewoldt RH, McKinley GH. On secondary loops in LAOS via self-intersection of Lissajous–Bowditch curves. Rheologica Acta. 2010;49(2):213–9.
67. Ewoldt RH, Winter P, Maxey J, McKinley GH. Large amplitude oscillatory shear of pseudoplastic and elastoviscoplastic materials. Rheological acta. 2010;49(2):191–212.
68. Kamkar M, Aliabadian E, Shayesteh Zeraati A, Sundararaj U. Application of nonlinear rheology to assess the effect of secondary nanofiller on network structure of hybrid polymer nanocomposites. Physics of Fluids. 2018;30(2).
69. Oo NB, Kumari N, Bhattacharya M, Abe R, Okamoto N, Pandey M, et al. Factors Influencing the Orientation of Carbon Nanotubes in Flexible and Lightweight Composite Ribbons during Direct Ink Writing. ACS Omega. 2025;10(24):25981–9.

70. Laurenzi S, Botti S, Rufoloni A, Santonicola MG. Mapping the residual strain of carbon nanotubes in DWCNT/epoxy nanocomposites after tensile load using Raman microscopy. Composites Communications. 2020;21:100424.
71. Shukla MK, Sharma K. Effect of carbon nanofillers on the mechanical and interfacial properties of epoxy based nanocomposites: A review. Polymer Science, Series A. 2019;61(4):439–60.
72. Hirth S, Cena L, Cox G, Tomović Ž, Peters T, Wohlleben W. Scenarios and methods that induce protruding or released CNTs after degradation of nanocomposite materials. Journal of nanoparticle research. 2013;15(4):1504.
73. Esmaeili A, Sbarufatti C, Ma D, Manes A, Jiménez-Suárez A, Ureña A, et al. Strain and crack growth sensing capability of SWCNT reinforced epoxy in tensile and mode I fracture tests. Composites Science and Technology. 2020;186:107918.
74. Habibur Rahman JM, Davis V, Gururaja S. Evaluating microstructural variation in nanocomposites via thermoelastic stress analysis. Journal of Reinforced Plastics and Composites. 2026;45(11-12):2448–63.
75. Tezel GB, Sarmah A, Desai S, Vashisth A, Green MJ. Kinetics of carbon nanotube-loaded epoxy curing: rheometry, differential scanning calorimetry, and radio frequency heating. Carbon. 2021;175:1–10.
76. Ramos PZ, Sarmah A, Green MJ, Richards JJ. In situ investigation of the rheological and dielectric properties of a cross-linking carbon nanotube-thermosetting epoxy. Soft Matter. 2023;19(32):6168–75.
77. Du F, Fischer JE, Winey KI. Effect of nanotube alignment on percolation conductivity in carbon nanotube/polymer composites. Physical Review B—Condensed Matter and Materials Physics. 2005;72(12):121404.
78. Park C, Wilkinson J, Banda S, Ounaies Z, Wise KE, Sauti G, et al. Aligned single-wall carbon nanotube polymer composites using an electric field. Journal of Polymer Science Part B: Polymer Physics. 2006;44(12):1751–62.
79. García-Tuñón E, Agrawal R, Ling B, Dennis DJ. Fourier-transform rheology and printability maps of complex fluids for three-dimensional printing. Physics of Fluids. 2023;35(1).
80. Hassanabadi HM, Wilhelm M, Rodrigue D. A rheological criterion to determine the percolation threshold in polymer nano-composites. Rheologica Acta. 2014;53(10):869–82.
81. Qu R-j, Wang Y, Li D, Wang L-j. Rheological behavior of nanocellulose gels at various calcium chloride concentrations. Carbohydrate Polymers. 2021;274:118660.